

Bioprinting: A review of processes, materials and applications



Bengi Yilmaz ^a, Ans Al Rashid ^{b,*}, Younss Ait Mou ^b, Zafer Evis ^c, Muammer Koç ^b

^a Department of Biomaterials, University of Health Sciences Turkey, Istanbul, 34668, Turkey

^b Division of Sustainable Development, College of Science and Engineering, Hamad Bin Khalifa University, Qatar Foundation, Doha, Qatar

^c Department of Engineering Sciences, Middle East Technical University, Ankara, 06800, Turkey

ARTICLE INFO

Keywords:
Bioprinting
Additive manufacturing
3D printing
Biomedical applications
Biomaterials

ABSTRACT

3D printing (3DP) processes have evolved from simple prototyping for visual inspection purposes to functional product manufacturing that offers flexibility, customization, scalability, reliability, durability, and relatively high speed. These processes have been successfully applied to the biomedical field by unraveling previously inaccessible freedom layers, such as increased design complexity. Bioprinting is one of the 3DP processes that has helped develop more advanced research-specific experimental tools and patient-specific therapeutic approaches. Given ongoing research progress in this field, a comprehensive review of existing achievements is vital. This review aims to present recent advances in 3DP processes with a particular focus on bioprinting. This study presents the history and development of bioprinting processes, the material developments in this field, and their applications. The selected bioprinting applications in the fabrication of 3D tissue-engineered constructs for bone, osteochondral, skin, and cardiac reconstruction are presented to demonstrate its potential in the further advancement of this multidisciplinary field of research and development.

1. Introduction

3D printing (3DP) processes have evolved from simple prototyping for visual inspection purposes to functional product manufacturing that offers flexibility, customization, scalability, reliability, durability, and relatively high speed. These processes have been successfully applied to the biomedical field by unraveling previously inaccessible freedom layers, such as increased design complexity. Bioprinting falls under the 3DP processes category that has helped to develop more advanced research-specific experimental tools and patient-specific therapeutic approaches. Bioprinting aims to manufacture living functional tissues and organs suitable for transplantation by combining living cells, scaffolds with 3D interconnected structures, and bioactive agents. Therefore, simultaneous processing of living cells and various biomaterials are needed in 3D bioprinting and its applications.

Ideal material for bioprinting must be biocompatible, i.e., induce appropriate host response specific for its intended application. It must also preferably be biodegradable to create space for and be replaced by newly synthesized tissue in time. The implanted material must provide the appropriate biological and biomechanical environments and biomechanical functions close to the native host within the body [1]. Standards are also critical to the advancement of science and

engineering in bioprinting. They should cover a wide range of activities, from simple laboratory procedures to the control of complex biological processes. The International Organization for Standardization (ISO) specified the nonclinical biocompatibility and medical device testing in the 'ISO 10993-Biological evaluation of medical devices' standard series. In particular, ISO 10993-1 provides the overall classification of medical devices. It gives algorithms for configuring the steps required in planning the study in which the biological safety of any biomaterial or medical device is determined [2]. However, there are still no standards addressing the bioprinting processes, production of biocompatible and bio printable materials (i.e., bio-inks), or characterization methods of the final products [3]. On the other hand, significant research efforts have been invested in transposing 3DP technology to the medical field, as indicated by the significantly increased publications (Fig. 1).

In addition to the scientific community's interest, commercial companies have also shown great interest in bioprinting. EnvisionTEC's Bioplotter [4] is the first commercial bioprinter that can produce tissue scaffolds from various biomaterials. The Chemical Institute of Sarria produced two different hydroxyapatite (HA) containing inks for 3D bioprinters [5]. Objet/Stratasys launched a transparent biocompatible photopolymer (MED610) [6], which creates rigid and transparent parts, such as surgical guides for a dental implant or orthopedic procedures.

* Corresponding author.

E-mail address: anrashid@hbku.edu.qa (A. Al Rashid).

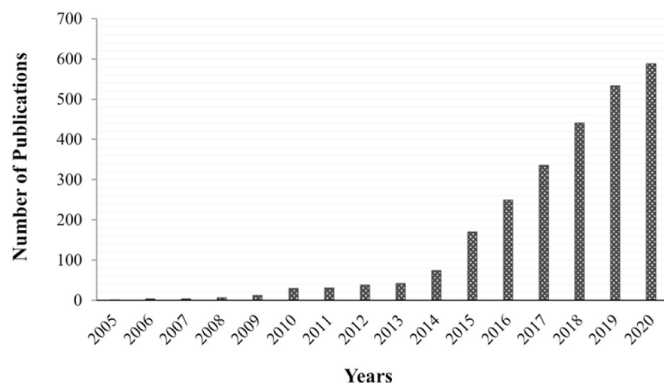


Fig. 1. Publication hits for “bioprinting” (data from Web of Science, accessed December 1st, 2020).

Autodesk teamed up with Organovo and developed commercial software for 3D bioprinting for the first time [7]. Organovo’s NovoGen MMX was considered the first commercial bioprinter tested for a fully cellular product [8].

Given ongoing research progress in this field, a comprehensive review of existing achievements is vital. This review aims to present recent advances in 3DP processes with a particular focus on bioprinting. This study presents the history and development of bioprinting processes, the material developments in this field, and their applications. The selected bioprinting applications in the fabrication of 3D tissue-engineered constructs for bone, osteochondral, skin, and cardiac reconstruction are presented to demonstrate its potential in the further advancement of this multidisciplinary field of research and development.

2. 3D printing processes & biomaterials

3DP processes utilize digital models obtained using 3D modeling software or digital scanning data. The designed models in computer-aided design (CAD) software are converted into an STL (standard tessellation language) file to represent objects in a three-dimensional cartesian coordinate system, storing information about objects' surface geometry, excluding color, texture, and other virtual model-related information. To be interpreted by the 3DP hardware (i.e., 3D printer), the STL file is further processed by a so-called “slicer software” to generate a machine-friendly file (.gcode file) [9,10]. The slicing software adds machine-specific extra information to the obtained slicing data. The ASTM/ISO standard defines terminologies used in 3DP technology and classifies the different 3DP techniques into seven sub-groups: material extrusion, material jetting, binder jetting, vat photopolymerization, powder bed fusion, directed energy deposition, and sheet object lamination [11]. Bioprinting processes have evolved from the traditional 3DP methods. Three out of seven generally classified 3DP processes have been implanted for bioprinting so far, as shown in Fig. 2.

3D printing materials are chosen according to the target application. 3DP processes are compatible with different material types: polymers, ceramics, metals, and composites. Polymers are often readily available and cost-effective, making them one of the most preferred strategies for 3D demonstration, prototyping, simulation, and actual applications [12], such as printing tissue scaffolds with PCL [13]. Ceramics, such as alumina, silica, and zirconia, are rigid ceramics that are hard to manufacture through conventional manufacturing processes. 3DP opened new and exciting perspectives in terms of manufacturing parts from ceramic materials. Biocompatible ceramics, such as hydroxyapatite (HA), can be processed with 3DP for biomedical applications. Ceramics have been successfully used as building materials for most 3DP technologies such as FDM [14–16] and SLS [17]. The majority of the load-bearing implants, such as artificial joints (for instance, a hip joint), spinal fixation devices, fracture nails, bone plates, and screws, and

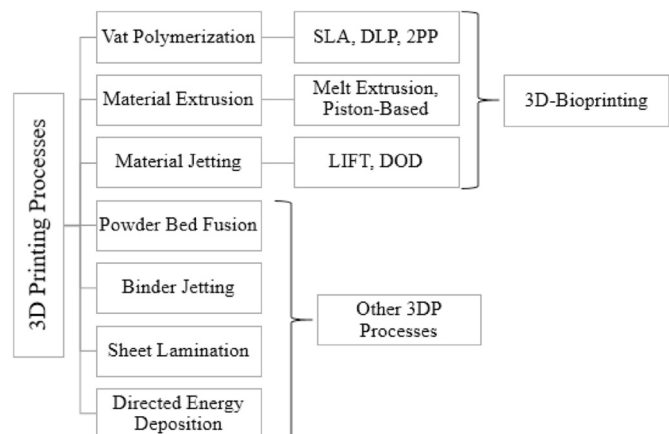


Fig. 2. Classification of 3DP processes and Bioprinting Processes.

dental implants, are fabricated from metallic biomaterials (e.g., titanium and its alloys, cobalt alloy, and 316L stainless steel), since they have good mechanical reliability [18].

Given the current advances in 3D printing technologies and materials, 3DP has found widespread use in biomaterials, regenerative medicine and tissue engineering, and laboratory device prototyping [19–21]. In the medical field, 3DP can also be used for aims such as teaching [22], functional flow modeling [23], procedural planning [24, 25], and device engineering [22]. Although 3DP medical applications are still in early-stage, past and current studies show promising results and imply a bright future for the field. One of the main advantages of employing 3DP in the medical field is its ability to produce patient-specific devices and therapeutic approaches. Some examples of materials used in 3DP are summarized in Table 1.

The working principles of all the 3DP processes and biomaterials involved are presented in the following sections. The subsequent text mainly comprise two main sub-sections, “section 2.1” presents the 3DP processes adaptation and modifications and biomaterials for bioprinting, while “section 2.2” presents other 3DP processes briefly for general biomedical sciences.

Table 1
Biomaterials for 3D bioprinting.

Material	Technology	Applications	References
Hydroxyapatite (HA) Poly(caprolactone) (PCL)	- Stereolithography - Inkjet/MJP	Bones and dental prosthesis	[26–35]
PCL Poly (lactic acid) (PLA) Poly (vinyl alcohol) (PVA)	- MJP - Stereolithography - BJ/3DP - FDM	Simulation and Surgical Planning	[23–25, 36–42]
Alginate Agar Gelatin Chitosan Hyaluronic acid PCL Poly (ethylene glycol) (PEG) Composites	- Inkjet - Micro-extrusion - Laser-assisted	Living Cells and Tissue Engineering	[12,43–64]
PCL PVA Ethylene-vinyl acetate (EVA) Poly (ethylene oxide) (PEO) Various Hydrogels	- Binder Jetting (BJ) - Inkjet/MJP - FDM	Drug delivery	[65–71]

2.1. Bioprinting

In 2004, the definition of bioprinting was presented in the first international workshop on bioprinting and bio-patterning. The term refers to using material transfer processes to design and assemble molecules, cells, tissues, and biodegradable biomaterials according to a specified configuration to perform one or more biological functions [72]. Bioprinting aims to manufacture living functional tissues and organs suitable for transplantation by combining living cells, scaffolds with 3D interconnected structures, and bioactive agents. Therefore, simultaneous processing of living cells and various biomaterials are needed in 3D bioprinting applications.

Standard 3D printing devices were first developed for rapid prototyping, rapid tooling for industrial manufacturing, and consumer product fabrication. These technologies' hostile environment makes them incompatible with 3D printing of living cells and many biological materials. Thus, limiting their biomedical applications to "passive" biological structures, such as bare scaffolds and highly porous substrates, which are often used as an adherence surface for cell growth and proliferation. Bio-friendly printing technologies have been developed to overcome these limitations. To date, vat polymerization, material extrusion, and material jetting technologies are adopted for bioprinting applications. 3D bioprinting devices can be designed as ink-jet, micro-extrusion, and laser-assisted systems [58], which corresponds to the mentioned standard 3DP processes. These technologies and material development for these processes are discussed here.

2.1.1. Vat polymerization (VP)

2.1.1.1. Stereolithography (SLA). Stereolithography (SLA), a vat polymerization method, was the first-ever introduced 3DP process [73]. In SLA, an ultraviolet (UV) range laser is used to induce polymerization of photopolymer resins (e.g., elastomers, epoxies, or acrylate) [74]. A pair of Galvano-scanners control the laser beam's lateral motion to improve printing speed and accuracy (Fig. 3). As a resin is used as the base material, the printing speed is tightly correlated with the light penetration and the curing depth, affecting new layer deposition. These parameters can be improved by modulating the resin viscosity, adding light absorbers, and polymerization facilitators.

Typically, SLA resins are made of polymers such as acrylates and epoxies. However, it is necessary to note that acrylate is not preferred for biomedical applications, given its cytotoxicity. Alternatively, novel biocompatible materials have been developed to overcome such material limitation issues, such as poly (lactic acid) (PLA) is an FDA-approved polymer [75]. The first use of SLA in the cell-containing bioprinting process was in 2004 [76]. An SLA vat was filled with Chinese hamster ovary cells and a photo-curable hydrogel consisting of poly(ethylene oxide) (PEO) and poly(ethylene glycol)dimethacrylate (PEGDM) and Irgacure was employed as a photo-initiator. The container was then

placed on a vertically moving table. UV light cured the places according to the design until the 3D structure was completed. The cell density was high with a laser intensity of 18 mW/cm^2 and wavelength of UV light of 365 nm. There is an increasing scientific interest in non-UV-based systems since UV can damage the DNA of encapsulated cells [77] and yield low post-printing cell viability. Lin et al. [78] developed a visible light-based projection SLA and used polyethylene glycol diacrylate (PEGDA) monomer to create hydrogel-based scaffolds with improved cell viability. Wang et al. [79] also used visible light-based SLA with a bio-ink consisting of PEGDA and gelatin methacrylate (GelMA) hydrogel with an eosin Y-based photo-initiator. This system produced a vertical 3D structure with 50 μm resolution and 85% fibroblast cell viability for the first five days.

2.1.1.2. Digital light processing (DLP). Digital light processing (DLP) also relies on UV light-induced polymerization of the resin. The significant difference between these two technologies resides in that DLP induces an instantaneous entire layer polymerization using digital micro-mirrors devices (DMD) [80,81]. In contrast, in SLA, a single laser point (e.g., layer pixel) is exposed at a time. As a result, DLP offers a higher printing speed than SLA and all other 3DP technology competitors (Fig. 3). The slicing data numerically control the DMD configuration. The applied light source has also evolved from standard lamps to light-emitting diode covering, thus, a more comprehensive range of wavelength at a lower cost [82]. The hardware setup for DLP offers higher lateral printing resolution. The z-resolution is tightly correlated with light penetration and scattering, which can be improved by adding light absorbers and polymerization facilitators. DLP achieves a resolution of about 1 μm (while the printing speed is about $30 \text{ mm}^3 \text{ s}^{-1}$) regardless of the layer's lateral area and complexity [83].

DLP can be employed with pure polymers (e.g., poly (lactic acid) (PLA) and poly- ϵ -caprolactone (PCL)) and composites containing ceramic and metal particles [84]. PLA resin compatible with the DLP method was synthesized and functionalized by methacrylic anhydride to produce hard tissue scaffolds with 600- μm pore size and 70% nominal porosity [85]. Seck et al. [78] fabricated the hydrogel scaffolds of poly D, L-lactide (PDLLA), and polyethylene glycol (PEG) by the DLP method. The scaffolds had a gyroid structure with pore sizes ranging from 387 to 558 μm with 15 μm layer thickness.

SLA and DLP are employed in the biomedical field to address various applications, including patient-specific models and functional parts, implantable devices, cell-free tissue engineering scaffolds, and cell-containing hydrogels [74]. Besides having high resolution, both SLA and DLP have the advantages of being cell-compatible techniques.

2.1.1.3. Two-photon polymerization (2 PP). Two-photon polymerization (2 PP) is another vat polymerization-based printing system like SLA and DLP, but it can provide better control and higher print quality [86]. Due to single-photon polymerization in SLA, the process occurs on the

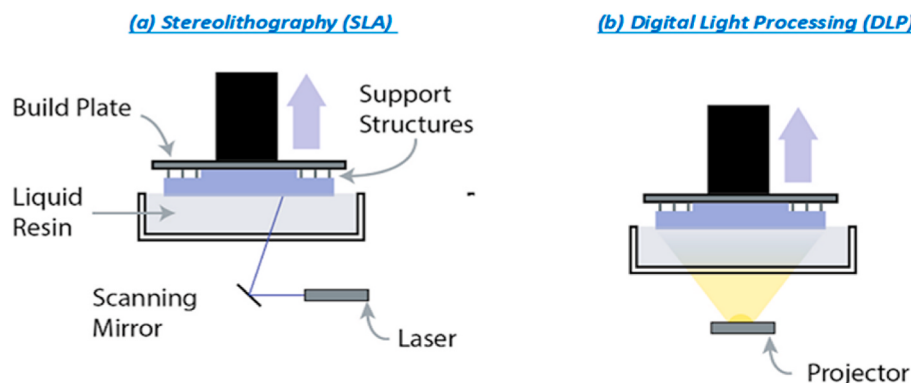


Fig. 3. (a) SLA and (b) DLP printers (Working Principle).

surface of a photosensitive resin that only allows building 3D structures layer by layer. On the other hand, in 2 PP, which uses near-infrared (NIR) femtosecond (Fs) laser pulses, the two photons are simultaneously absorbed by the photo-initiator. Allowing them to act as a single photon to initiate polymerization, enabling direct writing of any desired 3D model into the volume of photosensitive materials transparent in the NIR and highly absorptive in the UV spectral range [87].

The first use of the 2 PP technique for constructing 3D hydrogel structures containing living cells was reported in 2014 [88]. The human osteosarcoma cells (MG63) in the exposure region were reported to be damaged by the laser, while the others can survive. Therefore, to achieve acceptable post-printing viability of cells, it is also essential to identify and eliminate the source of photochemical cytotoxicity. Yu et al. [89] fabricated cell-free scaffolds of the photoresist by 2 PP containing PEGDA as the monomer and pentaerythritol tri-acrylate (PE-3A) cross-linker agent and reported that the minimum processing threshold was 2.94 mW and the feature line width of 80 nm was achieved.

2.1.2. Material extrusion (ME)

Fused Deposition Modeling (FDM), also referred to as fused filament fabrication (FFF), is the most commonly used material extrusion technique and was first developed in 1989 and patented by Scott Crump [90]. The FDM principle is based on material fusion (primarily plastics), extrusion, and deposition. Plastics are fed to the printer in filaments with diameters ranging from 1.75 to 3 mm (Fig. 4). The print head is equipped with a heating element and a nozzle with a small diameter (usually range from 0.1 mm up to 1.0 mm). The material is extruded from the printing nozzle upon melting to make a thin filament and then laid layer-by-layer on the build plate as specified by the “.gcode” file. The printing resolution is often tightly correlated with various parameters such as the nozzle's diameter, printing speed, and filament feed rate. As illustrated in Fig. 4, one head is dedicated to supporting material printing in such configurations, where the other is mainly used for model printing. Modern FDM printers can be equipped with dual (or multi) printing heads to print supporting materials for complex geometries. In addition, dual heads can be used for extruding multi-materials to fabricate functionally graded-materials.

FDM technology is often used with thermoplastics, such as poly(lactic acid) (PLA), polycaprolactone (PCL), poly(lactic-co-glycolic acid) (PLGA). Although there is a limited range of printable materials with FDM, this technique is essential due to being practical in easy material replacement, low maintenance expense, small size, and flexibility in operating temperatures [91]. Compared to other 3DP technologies, finished parts of FDM suffer from a low surface quality and

dimensional accuracy, limiting their use for various medical applications. Optimizing the 3D printing process by changing essential parameters, such as layer thickness, extrusion speed, and infill, must be considered to have an improved surface finish. However, several post-processing treatment methods, for example, sand polishing, chemical treatment with different solvents, such as acetone and methyl-ethyl-ketone, and vapor bath smoothening, can also be employed [92].

The FDM process itself can be applied directly in the biomedical area for the rapid casting of biomedical implants by using printed replicas [93], fabrication of prosthetic limbs [94] and radiotherapy patient simulators (phantoms) [95], 3D printing of microfluidic devices [96], sensors [97] and cell-free nanocomposite scaffolds [98], etc. However, materials extrusion processes are further modified and adopted for bioprinting. The most commonly used extrusion-based bioprinting process, namely, extrusion bioprinting (melt extrusion or piston-based), originates from FDM technology. The extrusion heads can be pneumatic, piston, or screw-driven systems. Landers and Muhlhaup [43] demonstrated the efficiency of using an extrusion-based system to construct 3D cell-laden hydrogels. The 3D extrusion bioprinting technique is based on a viscous cell-laden extrusion through a dosing needle (Fig. 5). Similar to conventional 3DP technologies, the needle position is numerically controlled based on a CAD model. The 3D structure is then built layer-by-layer. Many groups [44–46,99] have evaluated various hydrogels and composites to demonstrate the viability of 3D biological structures printed with this technology under multiple conditions.

Extrusion-based bioprinters can be modified to produce 3D structures composed of multi-walled and core-sheath fibers of different compositions using special nozzles with multi-compartments. Besides, it is also possible to adopt a microfluidic strategy to extrusion bioprinting [100]. Cell-laden bioinks, mainly composed of hydrogels and bioactive molecules, are dispensed by the printhead to create 3D structures. However, bioinks need to be designed by considering shear thinning or fast solidification properties for high-precision production.

2.1.3. Material jetting (MJ)

The technology shared by both polyjetting (PJ) and multijet modeling (MJM) is the two material jetting methods that were inspired by the conventional two-dimensional (2D) printing on papers. Like the traditional ink-jet printers, the printer head is equipped with drop-on-demand (DOD) ink-jet heads. When heat is applied to the DOD head's liquid ink, a small air bubble is formed and rapidly collapses, which results in a tiny droplet of ink being jettisoned out of the printhead through a small orifice. Piezoelectric actuators can also be used as alternatives to heat-induced bubble generation [101], which is particularly interesting and valuable in biomedical applications with sensitive temperature requirements. Material jetting printing technology has adopted a similar principle with modifications [102–104].

In MJM, the printing process is based either on simultaneous jetting

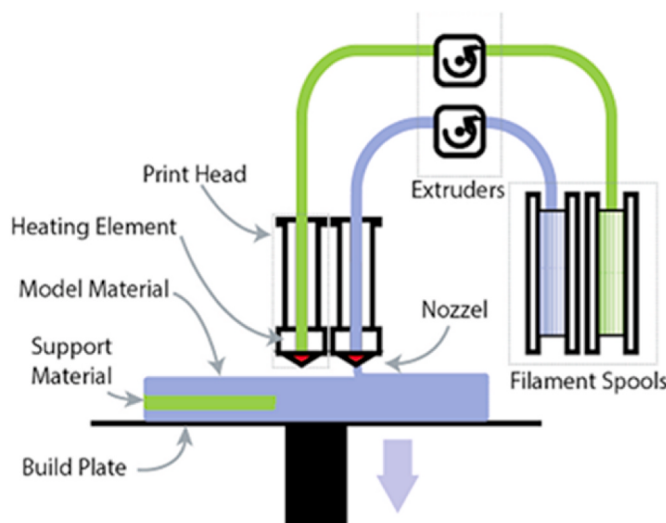


Fig. 4. Fused deposition modeling (working principle).

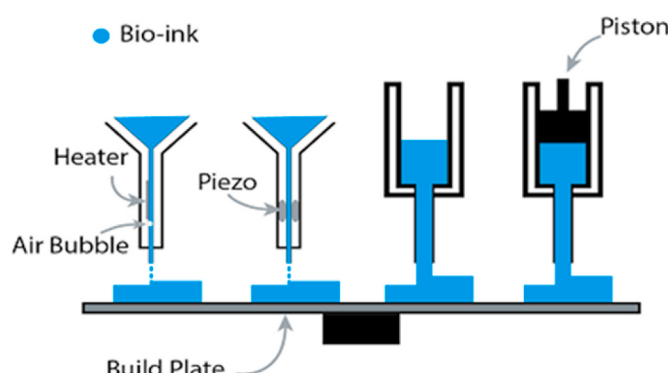


Fig. 5. Extrusion bioprinting (working principle).

of thermosetting resin and curing agent or, as proposed by Texas Instrument patents [105], based on wax melting at relatively low temperatures ($\sim 70^\circ\text{C}$) and rapid solidification upon contact with a cold substrate. PJ, on the other hand, is based on UV-curable photopolymers [102]. As illustrated in Fig. 6, material drops are deposited during each print head pass. A layer of material can be jetted per pass, or, for small print heads, only a fraction of a layer is jetted. In the second scenario, multiple head passes are required per layer, increasing printing time. Next, the build plate moves down one single layer height, and a new layer is jetted. This process keeps iterating until the object is constructed. A different head is used for overhanging regions to jet support material (Fig. 6; green). MJ, given their height accuracy [106], these techniques can be applied to medical model fabrication [107] and drug delivery simulation [65]. PJ technology is beneficial for multi-materials part printing. Thus, it allows for more realistic medical model segmentation printing. PJ technique can be sensitive enough to be used in 3D printing of small channels of microfluidic devices [108]. Two most commonly used MJ-based bioprinting techniques include drop-on-demand and laser-induced forward transfer.

2.1.3.1. Drop-on-demand (DOD). The first patent for ink-jet printing of living cells was obtained in 2006 by Clemson University's researchers [109]. Droplet-based ink-jet bioprinting is based on the ink-jet technology mentioned above. The most widely used ink-jet printer types use thermal and piezoelectric actuators to produce droplets in the DOD principle. The devices with a thermal actuation print head use an electric heating unit to form vapor bubbles that expand due to pressure and create a bio-ink droplet at the tip of the printhead. Since the process lasts only a few microseconds (about $2\ \mu\text{s}$), even if the temperature can reach $200\text{--}300^\circ\text{C}$ during the formation of a bubble, the printhead temperature only increases up to 10°C with minimal damage to the biological ingredients [110]. Ink-jet bioprinters with piezoelectric heads use voltage to induce a rapid deformation of the piezoelectric material. This deformation generates a pressure pulse in the fluid that forces the ink to drop from the nozzle. The droplet's shape and size can be varied by adjusting the voltage applied to the piezoelectric material.

2.1.3.2. Laser-induced forward transfer (LIFT). LIFT consists of a pulsed laser source, a focusing system, a ribbon target, and a receiving layer (substrate). The ribbon comprises a layer of material containing cells and a glass slide covered with an energy absorption layer, typically nano-thickness gold or titanium film [58,111]. A laser pulse evaporates the metal film to propel a jet of cells and molecules collected on the collector substrate [59]. LIFT method can precisely print cells on small-sized structures but require rapid hydrogels to obtain high resolution, resulting in low flow rates. Tissue engineering applications of a laser-guided direct writing system capable of arranging cells in spatially well-defined 3D arrays were reported in 1999 [112]. Such technologies allow printing complex biological structures such as mandible and

calvarial bone, cartilage, and skeletal muscle [113]. Although laser-guided direct writing system bioprinting systems are not commercially common, they have many advantages, such as high spatial resolution and printing various biological materials, and providing high cell viability.

2.2. Other 3DP processes

2.2.1. Binder jetting (BJ)

Binder Jetting (BJ), also known as 3D powder binding technology, relies on powdered material (e.g., alumina, etc.) binding by the mean of binder material (e.g., colloidal silica, etc.) jetting [114]. This technique is similar to conventional ink-jet printing, and traditional ink-jet printing heads are often employed in BJ without further modifications. The printing process starts with the dispersion of a thin layer of powder on the build plate. The print head jets droplets of binding material on specific regions based on the CAD model. The binder induces powder particles to fuse, forming a solid layer. Before the full cure of a layer, the build platform steps down a few microns ($\sim 0.1\text{ mm}$), and a new layer is dispersed by a dispersing roller (Fig. 7). The process iterates over until the solid object is entirely constructed. The unbound powder can be used as a supporting structure for overhanging regions in the model and recycled upon job completion. Often, a build object requires significant post-processing steps such as sintering or resin infiltration to improve surface finish and mechanical properties.

BJ is mainly used for pure prototyping and demonstration purposes. However, since it is based on ink-jet technology, BJ can produce high-fidelity models with multiple colors within individual layers. This advantage makes BJ the most preferred approach for 3D visualization, planning, and conceptual modeling, particularly in surgical procedures. BJ technology can be subdivided into two categories, namely, powder-based binder and ink-based binder. In the powder-based binder, the binding agent is embedded within the powder particles (PLA, PLGA, PCL). When exposed to an aqueous or organic solvent, the powder particles swell and fuse by polymer inter-diffusion and entanglement.

On the other hand, the ink-based binder is mainly preferred for constructing an object from metallic or ceramic powder particles. In this configuration, the ink-jet head dispenses inorganic (e.g., colloidal silica) or organic (e.g., polymeric resins and polymer emulsions) binder on the powder particles. The binder firmly binds particles together by forming a thin adhesive film upon drying. Alternative binding agents, such as citric acid, showed convincing results when used with HA powder, used for bone tissue scaffold fabrication in RM [26,27].

BJ can also be utilized for the manufacturing of other bioceramics. Mancuso et al. [115] prepared different glass-ceramic formulations of apatite–wollastonite and silicate-based glasses blended with maltodextrin powder as a binder to form micro-and macro-porous bone scaffolds for load-bearing applications, and they obtained TE constructs which have Young's modulus equivalent to the cortical bone after sintering up

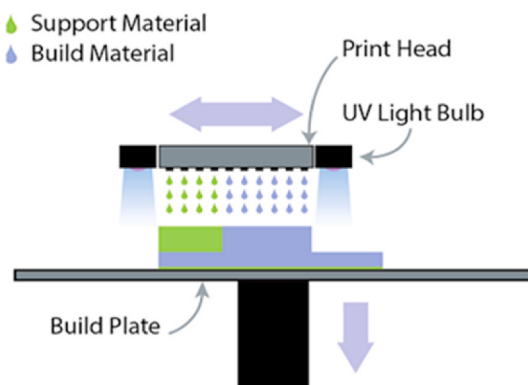


Fig. 6. Material jetting (working principle).

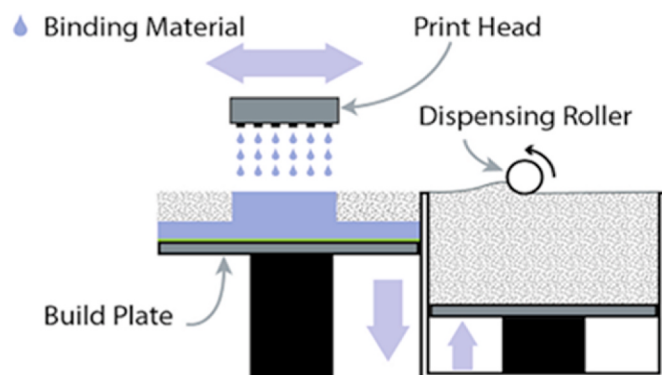


Fig. 7. Binder jetting (working principle).

to 1250 °C.

BJ is one of the 3DP techniques that is also compatible with biodegradable metals. Hong et al. [116] used BJ-3D printing followed by binder burn out and subsequent sintering to fabricate biodegradable bone tissue engineering scaffolds from Fe, Mn, and Ca powder mixture. The corrosion rate of 3D-printed alloys was reported to be greater than that of the sintered compact pellets, attributed to the micropores after binder burn-out. However, the micropores can also improve osseointegration. 3D printed Fe–Mn-based alloys using the BJ method are also studied for craniofacial biomaterial applications [117].

2.2.2. Powder bed fusion (PBF)

Powder bed fusion processes are further classified based on the fusion mechanism as; Selective laser sintering (SLS), selective laser melting (SLM), and electron beam melting (EBM). SLS is similar to BJ since it is also based on bonding the powdered material. However, as opposed to BJ, SLS technology uses a focused laser beam to induce layer-by-layer local sintering of the powder particles to form a 3D object (Fig. 8).

The principle of SLS consists of powder dispersing on a build plate, a numerically controlled focused laser, primarily CO₂ and Nd:YAG [118], is then used to induce the powder particles fusion (i.e., powder solidification), then, the build plate is lowered by a single layer height, and the process starts again. With laser scanning in SLS, the powder particles partially melt and re-solidify, while in SLM, the powders completely melt [119]. In EBM, the melting process's energy source, i.e., the scanning process, is an electron beam emitted from a tungsten filament [120]. The process steps are repeated over and over until the final object is reconstructed. The unprocessed material is kept being used as a support for overhanging regions in the model. The container chamber is kept at an elevated temperature to improve the curing process and decrease processing time. Ideally, the chamber temperature is kept just below the material softening point. SLS printing technology allows the use of a wide range of materials with specific mechanical properties, such as parts that are subject to significantly high mechanical loads. The printing resolution and surface finish in SLS are tightly correlated with the powder particle size, shape, and density [121]. Thus, one can improve the surface finish and reduce the post-processing steps by reducing the powder particle size [122,123]. The particle size also affects the density and mechanical properties of the finished product [124].

Powder bed fusion (PBF) techniques have significant advantages in implant fabrication over other 3DP approaches. These methods are the most straightforward methods of 3D printing for producing porous orthopedic implants directly, and porosity is one of the most critical features for bone-in growth and improved osseointegration of metallic biomaterials. Additionally, SLS, which applies to polymers, metals, and alloy powders, and SLM and EBM compatible with specific metallic materials, can fabricate scaffolds and implants with complex geometries and open cellular structures [119].

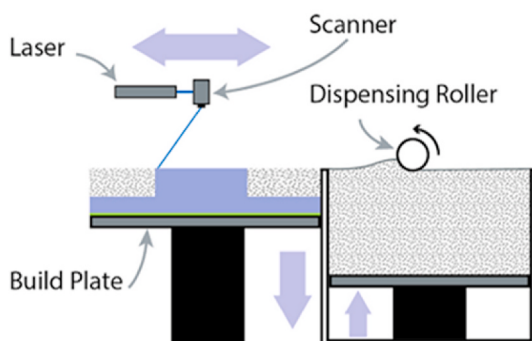


Fig. 8. SLS printer (working principle).

Ceramics, metals, composites, and pure polymers were employed as model materials for end-user manufacturing and prototyping parts [125–128]. The hostile environment (e.g., high temperature) imposed by this technology makes it incompatible with the bioprinting of living cells and bioactive molecules. However, SLS technology can still be employed in biomedical applications oriented toward bone grafting and scaffold printing. In these applications, polyesters such as poly(caprolactone) (PCL) [28] and poly(lactide-co-glycolide) (PLGA) [29] are often used in combination with calcium phosphate (CaP) particles [30,129].

3. Bioprinting applications

3D bioprinting technologies have found extensive applications in the biomedical area, including skin (for example, full-thickness skin substitutes or wound dressings), orthopedic, dental, osteochondral, cardiovascular, and other soft tissue engineering applications (for example, pancreas and liver).

3.1. Bone tissue engineering

Bone is the second most transplanted organ globally, and more than four million surgeries are performed each year to treat bone defects [130]. Autografting and allografting techniques are still the leading solutions in bone repair. Using an autograft is an expensive and invasive option and may cause infections and hematomas that frequently affect both donor and surgical sites. Besides, allografts have problems such as the possibility of causing an immune reaction and subsequent rejection by the host tissue; the patient may also be infected if the graft is contaminated [131].

Biomaterials and engineered structures have become increasingly important in bone tissue replacement. Several techniques that have previously been used to build TE structures have not been efficient to provide vascularity, which is one of the most critical factors affecting the success of the structure in the body. Prolonged biodegradation processes can occur when bulk materials are used, and this can cause inflammation reactions. Electrospun nanofiber-based scaffolds of various natural and synthetic polymers have been developed to mimic the extracellular matrix (ECM). These structures generally do not have enough strength to eliminate mechanical mismatch with bone tissue [132]. The difficulties encountered in TE constructs' production while meeting the clinically required size, necessary structural support requirements, osteoinductivity, and controlled biodegradability [133]. Since all of these requirements cannot be fully met by other scaffold production methods, bioprinting has received considerable focus within bone TE due to its tightly controlled computer-driven fabrication.

Ceramic scaffolds (such as CaPs and Bioglass) are preferred for their biocompatibility, high mechanical strength, controllable biodegradability, and intrinsic osteoinductivity in hard tissue replacement applications. Still, they are not usually used in bulk form due to their high brittleness. Instead, they are used with biocompatible polymers as composites, improving the mixed polymer and ceramics' physical properties in the final product and printability during the bioprinting process. Scaffolds can be printed using ceramic powders (e.g., HA and alumina) combined with polymers such as PCL and PLA [26]. For instance, previous studies have demonstrated that combining PCL with nano-particles reduces its toxicity [51] allowing, thus, its usage as a printing substrate [52]. PCL and PLA were both successfully used to 3D print porous structures, making them preferred for bone scaffolding applications, but a diverse range of polymeric materials available for bioprinting technology. Table 2 lists some examples of 3D printed composite biomaterials for engineered bone tissues and their osteogenic potential.

Composites consisting of bioceramics can also be 3D-printed via various techniques other than material extrusion, such as laser-assisted sintering and direct writing-based processes. For example, Ramu et al. [139] fabricated bone scaffolds with interconnected cubical and

Table 2

3D printed composite biomaterials for bone tissue engineering.

Biomaterials ^{a,b}	Cells	Fabrication method	3D Printer	Main outcomes about osteogenic potential ²
PCL- Ca ²⁺ -polyP microparticles (at a 2:1 w/w ratio) [134]	Human primary osteogenic sarcoma (SaOS-2) cells	Pneumatic melt extrusion	3D-Bioplotter, Envision TEC, Germany	<ul style="list-style-type: none"> More living SaOS-2 cells were identified on the PCL/Ca-polyP-MP scaffold compared to the plain PCL scaffold after 3 days of cultivation. The hybrid material was showed to upregulate the steady-state-expression of the cell migration-inducing chemokine stromal cell-derived factor-1α (SDF-1α).
PLA(10 wt%)- β -tricalcium phosphate (β -TCP) (5 wt %) with four different hydrogels: collagen, sodium alginate, halamomas levan, and chitosan (1 wt % concentration ratio, individually) + amoxicillin (0.5 wt% as an antibacterial agent in chitosan added blend) [135]	Human primary osteogenic sarcoma (SaOS-2) cells	Syringe extrusion	Hyrel 3D, USA with SDS-5 extruder	<ul style="list-style-type: none"> The metabolic activity of cells and adhesion was highest on chitosan added scaffold, followed by halamomas levan added scaffold. The presence of amoxicillin negatively affected the cell viability.
Pure PCL; PCL- silanated silica particles (5, 10, 20 wt %) [136]	Human osteoblast-like cells (MG-63)	Pneumatic melt extrusion	Not specified	<ul style="list-style-type: none"> Calcium mineralization of cells and cell proliferation rate on the PCL-silica (20%) composite scaffold was 2.9 and 1.7 times greater than that of the pure PCL, respectively. Other osteogenic differentiation results (ALP activity and qRT-PCR) also indicated that the addition of silanated silica particles increased bone mineralization with a high level of mRNA expression compared to pure PCL.
HAp/ β -TCP (at a mass ratio of 60/40) (67% w/w)-20 wt% Pluronic F-127 solution (33% w/w) as 3D printed biomaterial and RGD-phage nanofibers (10 ¹⁴ pfu/ml) and chitosan (1 mg/ml) as coating material [137]	Mesenchymal stem cells (MSCs)	Extrusion	RoboCAD 3.0 robotic deposition device, 3-D Inks, USA	<ul style="list-style-type: none"> Cell-seeded scaffolds were evaluated with radial defect model on Sprague Dawley rats. The formation of new bone was confirmed 8 weeks after implantation by histological analysis and microcomputed tomography (micro-CT) of RGD-phage containing scaffolds.
Nano-sized HA-p-chitosan-silica (15/50/35 M ratio, respectively); Chitosan-silica (50/35 M ratio, respectively) [138]	Mouse bone mesenchymal stem cells (mBMSCs)	Pneumatic syringe extrusion	3D-Bioprinter, Regenovo, China	<ul style="list-style-type: none"> The cells on HA containing scaffolds displayed a significantly higher proliferation rate and calcium mineralization than that on the HA-free chitosan-silica scaffolds after 7 days of incubation, but there was no significant increase in ALP activity after 14 days.

^a Different biomaterial formulation are separated with semicolons () .^b Material Abbreviations: PCL-poly(ϵ -caprolactone); polyP- poly(phosphate); PLA-poly (lactic acid); β -TCP- β -tricalcium phosphate; ALP-alkaline phosphatase; RGD-Arg-Gly-Asp peptide.

spherical pores with 40–70% porosity using the SLS method with different polyamide and HA mixes. On the other hand, direct printing of dense pure ceramic parts is often challenging due to the extremely high melting temperature of ceramics. Additionally, it's challenging to get the designed scaffolds using direct 3D printing due to ceramics' shrinkage during sintering [140]. Nevertheless, various research groups continuously evaluate novel strategies to overcome these limitations with encouraging results while maintaining a sustainable manufacturing process [141–143].

Table 3 lists some selected examples of 3D printed metallic biomaterials for bone tissue engineering to demonstrate 3DP techniques' diversity and direct writing 3DP compatible metallic biomaterials. The internal micro and nano-architecture of a cellular (porous) scaffold structure significantly affect its mechanical properties and *in vitro/in vivo* biological behaviors. Recent advances in bioprinting have enabled rapid and accurate production of cellular structures based on 3D CAD models. Since the unit cell geometry and dimensions can control the final product's mechanical performance, producing cellular structures with cortical and cancellous bone-equivalent stiffness and strength while maintaining the optimum cell adherence, proliferation, and differentiation is a great scientific interest now. Fig. 9 depicts some unit cells and lattice structures used in 3DP for bone graft applications (see Table 4).

This type of CAD-designed controlled porosity can be applied to all material classes with a careful selection of bioprinting methods and printing process parameters to tailor the mechanical and biological performance. Limmahakun et al. [151] fabricated 3D cellular structures (octahedral, pillar octahedral, cubic, and truncated octahedral) with precisely controlled internal architectures for bone TE by using

photopolymerizable polymer (VisiJet®M3 Crystal) consisting of urethane acrylate oligomers and ProJet®3500SD (3D Systems, USA) equipment. The pore size was 40–550 μ m, and high porosity of 74% has been achieved. Strut alignment of $\pm 45^\circ$ was reported to increase the adherence of murine pre-osteoblastic cells (MC3T3-E1).

Additionally, post-processing and surface modifications methods are essential in creating much smoother surfaces than the as-built ones and removing the residuals, especially for powder-bed fusion 3DP techniques, such as SLM and SLS. These kinds of treatments are also crucial to change the internal structure of the material. Yan et al. [152] manufactured a gyroid triply periodic minimal surface (TPMS) lattice composed of Ti6Al4V alloy by using SLM. While the as-built lattices exhibited an out-of-equilibrium microstructure with very fine α' martensitic laths, they showed a homogenous and equilibrium lamellar $\alpha+\beta$ microstructure with less dislocation and crystallographic defects after heat treatment at 1050 °C for 4 h followed by furnace cooling. The sandblasting of 3D printed parts was reported to remove metal particles successfully but created tiny cracks, which were later eliminated by hydrochloric acid (HCl) etching. Subsequent sodium hydroxide (NaOH) etching was reported to result in many small and shallow micro-pits and developed a sodium titanate hydrogel layer on the lattices' surfaces, improving bioactivity Ti alloy and deposition of HA in simulated body fluid (SBF).

Bioprinting of CAD-designed hard-tissue structures customized to specific patient needs can allow the rapid production of large amounts of samples and improve routine clinical procedures for products that better meet regular surgical needs. However, commercial translation of advanced systems, such as cell-laden tissue constructs, needs tissue maturation by dynamic cell culture in bioreactors.

Table 3

Metallic Biomaterials in 3DP for the restoration of Bone.

Biomaterial	Fabrication method	3D Printer	Total porosity (vol%)	Pore Shape and Size	Post-Processing Method
Ti6Al4V alloy [144]	Selective laser melting (SLM)	M2, Concept laser, Germany	<ul style="list-style-type: none"> Designed porosity: 66.1–79.5 Measured porosity: max 7.9% different than the designed porosity 	<ul style="list-style-type: none"> Diamond-like Max measured pore size = 650 ± 20 μm 	Surface bio-activation: First acid pickling in 0.7%wt hydrofluoric acids for 10 min and subsequent HA coating by electrochemical method.
Ti6Al4V alloy [145]	Selective laser melting (SLM)	DMP ProX 320, 3D Systems, USA	<ul style="list-style-type: none"> Designed porosity: 53.9–88.1 Measured porosity: 49–87 	<ul style="list-style-type: none"> Gyroid structure Pore size of printed parts was not measured, unit cell size = 4 × 4 × 4 – 6 × 6 × 6 mm³ 	As-built samples were cleaned by sonication for 15 min in DI water, no post-processing applied.
Ti6Al4V alloy [146]	Selective laser melting (SLM)	M2, Concept laser, Germany	<ul style="list-style-type: none"> Designed porosity: 60–80 Measured porosity: 58.01–78.85 	<ul style="list-style-type: none"> Diamond, gyroid, orthogonal, truss and cube Pore size was about 500 μm for gyroid structure as determined from scanning electron microscopy (SEM) images. 	3D-printed parts were heated for 4 h to 1000 °C with a heating rate of 4.08 °C/min in a vacuum furnace and then cooled to room temperature.
Ti6Al4V alloy [147]	Electron beam melting (EBM)	Arcam A1, Arcam, Sweden	<ul style="list-style-type: none"> Designed porosity: 72–74 Measured porosity: 82–85 	<ul style="list-style-type: none"> Gyroid CAD-design pore size was 0.85, 1.06 and 1.27 mm for 3 different group while the measured values were 1.85, 1.25 and 1.5 mm, respectively. 	As-built parts were blasted to remove the remaining powder particles and were machined to the final dimension by electrical discharge machining (EDM).
Titanium (Ti) [148]	Selective laser melting (SLM)	SLM 50, Realizer GmbH, Germany	The measured overall open porosity was 62 or 80 for different designs and 58/77 for core-shell cylinders.	<ul style="list-style-type: none"> Diamond Pore sizes of 200 μm, 500 μm and 200/500 μm (for core-shell cylinder) are CAD-designed and max standard deviation was 2.4% in diameter for printed parts. 	Chemical polishing with hydrofluoric acid solutions (1%–5% HF) for 1–6 min and in mixtures of hydrofluoric and nitric acids (2.0/20%, 1.3/9.0%, 4.0/16%, 2.2/20% HF/HNO ₃ respectively) for 3–9 min.
CoCrMo alloy [149]	Selective laser melting (SLM)	MYSINT100, SISMA, Italy	<ul style="list-style-type: none"> Designed porosity: 60–80 Measured porosity: 58.01–78.85 	<ul style="list-style-type: none"> Trabecular, circular, crossing rods Pore size of printed parts were not measured, mean trabecular spacing was set to 670 μm for trabecular design. 	After sintering, the samples were cleaned via high-pressure air jets and ultrasound.
We43 magnesium alloy [150]	Selective laser sintering (SLS)	Laboratory SLM setup consist of single mode ytterbium fiber laser (IPG YLR-200) with 230 W maximum output power, a galvanometric scanner (SCANLAB hurrySCAN 20) and a f-theta focusing lens (SILL S4LFT 3254/126)	<ul style="list-style-type: none"> Designed porosity: 67 Measured porosity: 64 	<ul style="list-style-type: none"> Diamond Pore size of 600 μm was used in the design, min pore size of as-built samples was about 500 μm. 	The samples were chemically polished for 2 min in a solution of hydrochloric acid (5 vol% HCl), nitric acid (5 vol% HNO ₃), and ethanol (90 vol% C ₂ H ₅ OH).

3.2. Osteochondral tissue engineering

Cartilage defects are usually caused by trauma, illness, or aging. The defects disrupt the joints' biomechanical properties, affect the tissue's performance, and may result in disability. Most cartilage defects are often accompanied by osteochondral lesions involving both the hyaline cartilage in the joint and the underlying subchondral bone. It is desirable to provide simultaneous regeneration of the different layers of the osteochondral lesion. However, due to the different biological origins and chemical composition of cartilage and subchondral bone in osteochondral injuries, treatment with existing clinical techniques, such as medication and surgical intervention, remains a major challenge.

Knee cartilage treatment applications can be categorized as arthroscopic chondroplasty, autologous chondrocyte transplantation, osteochondral graft transplantation, cell-based cartilage regeneration, implants, and microfracture application. These approaches may lead to total joint prosthesis surgery as the last stage intervention. Some of the current treatment options, including absorbable 3D scaffolds for cartilage regeneration, are depicted in Fig. 10.

3DP methods are also prominent for osteochondral scaffold fabrication due to their ability to produce interconnected porous scaffolds with well-controlled pore geometries as the scaffold structure can be designed to exhibit tissue-matched mechanical properties. Various 3DP techniques have been used for osteochondral tissue regeneration, including liquid, powder, and solid-based methods to create gradient

scaffolds with various biomaterials, structural properties, and mechanical properties [154].

Osteochondral tissue engineering requires more complex designed scaffolds than bone scaffolds. For example, articular cartilage is attached to the subchondral bone, and thus the osteochondral unit at the knee is formed. Therefore the natural structure is multi-layered and includes tissues with different characteristics. The complex, non-linear, viscoelastic, anisotropic, and heterogeneous structure and composition of the cartilage make it necessary to produce scaffolds corresponding to this structure by innovative bio-fabrication methods biomaterials that can provide a biomimetic environment. Today, 3D printing and bioprinting strategies allow the fabrication of scaffolds and biological tissue substitutes that can accurately reflect the complex organizational structure and material properties of tissues and organs. In the table below, examples of multilayer and/or bi-phasic osteochondral tissue scaffolds created with 3D printing techniques are given.

Barbeck et al. [158] combined the PLA layer and a biphasic PLA/bioglass G5 layer for regeneration of osteochondral defects by using a nozzle-deposition system (direct-printing tool) (Tissue Engineering 3-Dn-300, Sciperio/nScript Inc). The authors reported that the data obtained from both histological observations and histomorphometric measurements revealed the tissue responses to different layers of two-layered scaffolds are localized to the relevant implantation sites.

Table 4

Examples of 3D printed bi-phasic/multilayer osteochondral tissue scaffolds.

Biomaterials and structure	Fabrication method	Outcomes about mechanical properties
nfrapatellar fat pad derived stem/stromal cells (FPSCs) and chondrocytes-loaded RGD-alginate hydrogels in the chondral layer, In the bone forming layer, PCL frames used to mechanically strengthen bone marrow derived stem cell (BMSC) loaded RGD-alginate hydrogels in both layers. Agarose hydrogels and PLGA and PLA polymers were also used in the study [155]	Thermal assisted extrusion printing technique (70 °C for PCL)	There was no change in the PCL filament diameter (0.22 ± 0.03 mm) and the mechanical properties of 3D printed PCL supports at 28 days <i>in vitro</i> . On the other hand, PLGA (with lactic acid to glycolic acid ratio of 65:35) did not provide sufficient mechanical reinforcement, with the Young's modulus reducing from 7.17 MPa to 0.0075 MPa 3D printed structures of PLA and PLGA (85:15) experienced relatively less dramatic changes in mechanical properties over time in culture. The mechanical properties of the copolymer hydrogels obtained are as follows: tensile strength (0.41 MPa), high elasticity (up to 860% stretching) and high compressive strength (up to 8.4 MPa).
[N-acryloyl glycaminide-co-N-[tris(hydroxymethyl) methyl] acrylamide (THMMA)] copolymer hydrogel (PNT) with transforming growth factor beta 1 (TGF-β1) in upper layers and β -TCP particles in lower layers [156]	Thermal assisted extrusion printing technique (70–75 °C)	
Osteogenic peptide/β - TCP/PLGA in the bone part, Thermal-responsive poly(D,L-lactic acid-co-trimethylene carbonate) (P(DLLA-TMC)) frame on top of the subchondral layer to provide bonding strength between the cartilage layer and the subchondral layer, In the cartilage part, collagen-I hydrogel containing TGF-β1 is added to the macropores of this frame [157]	Lyophilization after cryogenic extrusion printing technique (-30 °C)	The shear strength between the cartilage layer and the subchondral layer was measured as 0.4 MPa at 37 °C. The osteochondral interface also showed a peel strength of 470 N/m at 37 °C.
Two-layered 3D printed scaffold combining PLA layer with 5% PEG and PLA/G5 bioglass layer also containing PEG [158]	Thermal assisted extrusion printing (40 ± 5 °C)	While PLA scaffolds had compression modulus around 28.38 ± 3.99 MPa, PLA/bioglass scaffolds showed values around 44.19 ± 2.67 MPa. Mechanical strength of bi-layered structures has not been reported.
Gelatin methacrylate (GelMA) -polyethylene (glycol) diacrylate (PEGDA) -nanocrystalline hydroxyapatite (nHA) in the subchondral bone part of the scaffold GelMA-PEGDA-TGF-1 loaded PLGA nanoparticles to form the cartilage part [159]	Stereolithography (SLA) printing	The compression module of the GelMA-PEGDA control group was significantly lower than the other groups due to the absence of nHA in this group. The Young's modulus of the layer formed by PLGA nanoparticles loaded with GelMA-PEGDA-TGF-1 was measured around 2.25 MPa.

3.3. Skin tissue engineering

The body's outermost layer is the integumentary system that consists of the skin and its appendages: hairs, nails, sweat, and sebaceous glands. The skin has many protective and regulatory functions, such as serving as a barrier to infectious organisms, resisting potential hazards from harmful substances, regulating body temperature, and acting as a sensory interface with the environment. However, the skin is susceptible to a wide range of infections, damages, and illnesses like cancer as the outermost organ.

The skin has an intricate design that varies in different parts of the body, but it is mainly composed of a highly vascular dermis covered by multiple layers of cells known as the epidermis. When the skin is injured or its integrity is broken for other reasons, organic residues should be removed, and the wound area should be supported by adding new components. These should include extracellular matrix and soluble factors to rebuilt cellular interactions. The autologous skin grafts are ideal wound closure materials used in acute and chronic wound deficiencies with different etiologies. However, other solutions, such as bioengineering and synthetic alternatives, are necessary as skin grafts can lead to issues, such as additional health risks and deforming donor site morbidity, and unavailability of good healthy skin should also be considered.

Tissue-engineered skin substitutes and other wound dressings are designed to replace or support the skin's form and function permanently or temporarily until the integrity and function are recovered. An ideal skin substitute should not cause decreased sensitivity, scarring, skin discoloration. It should resist infections, prevent dehydration, and mimic the natural skin tissue's elasticity.

Many production techniques, such as electrospinning, freeze-drying, and solvent casting, have long been used for skin substitute constructions. Skin bioprinting has gained increasing attention due to its ability to provide sophisticated and controlled production that is impossible with traditional skin graft production methods. It is among the most rapidly developing biomedical applications of 3DP technologies.

Vijayaventkaraman et al. [160] emphasized a tremendous demand for 3DP technology companies because there is a huge potential for immediate commercialization. They gave three examples from 2015: 1)

L'Oréal USA collaborated with Organovo, Inc. to 3D bioprint skin tissue models for testing the cosmetic products. 2) Procter & Gamble (P&G) started a research project in Singapore to collaborate with biomaterial scientists and tissue engineers for developing skin models. 3) Rokit, the market leader in 3D printing technology in Korea, announced that their focus would be on the bioprinting of human skin tissue in a government-funded project. As 3DP technology in skin TE becomes widespread over time, similar examples are continually increasing.

Patient-specific production is one of the essential advantages of 3DP technologies. For example, Albanna et al. [161] developed a mobile skin bioprinting system that provides rapid on-site management of extensive wounds (Fig. 11). The system's main components consist of a hand-held 3D scanner and a printhead with eight 260 μm diameter nozzles, each driven by an independent dispensing motor that enables XYZ movement coordinates.

The number of research studies on skin regeneration related to the use of both bottom-up and top-down 3DP technologies by the scientific community is far greater than the number of commercial products. The number of research articles on full-thickness skin models, which resemble natural human skin, has increased in the literature, especially

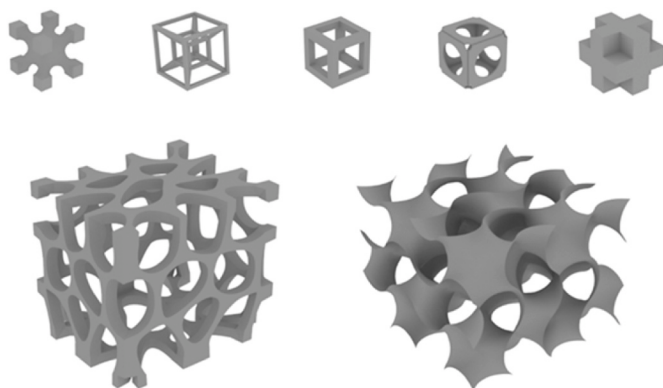


Fig. 9. Different designs of unit cells (upper pane) and gyroid (Voronoi) lattice structures (lower pane) used in bone tissue engineering.

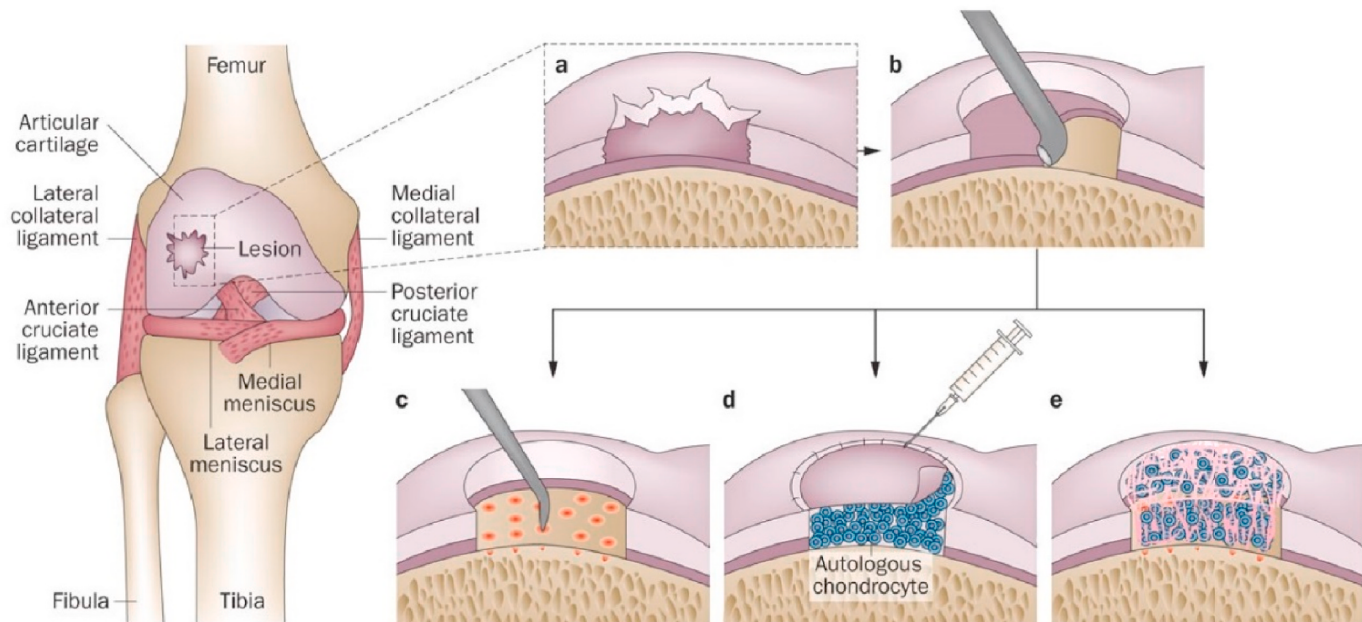


Fig. 10. Current treatment options for cartilage regeneration.

(a) A full-thickness chondral lesion. (b) The defect is debrided to remove damaged cartilage and bone to create a healthy border which enables improved tissue integration. (c) Microfracture drills into the subchondral bone to create channels that allow a blood clot to form in the defect. (d) Autologous chondrocyte implantation uses chondrocytes which are inserted into the defect and covered with a periosteal patch or a collagen membrane. (e) Matrix-induced autologous chondrocyte implantation, chondrocytes are cultured in vitro and seeded onto an absorbable 3D scaffold, then implanted into the defect, and fixed to the defect with fibrin glue. Reproduced with permission from Ref. [153].

in recent years. It has been shown that skin is one of the most suitable organs for restoration using 3DP technology in the medical field. Table 5 summarizes some recent examples of 3DP manufacturing of skin tissue-engineered products.

3.4. Cardiovascular tissue engineering

Like standard product prototyping and fabrication with 3DP, cardiovascular 3DP starts from a 3D model, which is then translated into a machine instructions-set to perform a layer-by-layer fabrication of the object (i.e., organ). The patient-specific organ's 3D model is often obtained from medical imaging technologies that generate a volumetric imaging dataset. For instance, Computerized Tomography (CT) scans, volumetric 3D echocardiography, Cardiac Magnetic Resonance (CMR), and 3D Trans-Esophageal Echocardiography (TEE) can all be used to obtain a full or partial patient organ 3D reconstruction [20]. Because of its high spatial resolution (sub-millimeter), CT has been the primary imaging methodology employed for high fidelity, patient-specific organ, and tissue imaging for 3D applications [41,42]. Following the image acquisition, the obtained results are usually segmented to distinguish various organ components, and last, the segmented images are re-rendered in 3D before conversion to “.stl” files. However, it is to note that although the obtained models can be used as-is for 3D printing, complex anatomical models often need extra final touches using CAD software, which might be the case in situations where the segmentation targeted complex vascular network or for device insertion adaptations (e.g., aortic stent simulation).

3DP could also be used as a diagnostic tool for patients with structural heart disease [32]. Moreover, SLA has been used *in-vivo* and *in-vitro* to build patient-specific mitral valves from elastomeric polymers [39].

Recently, Ware et al. [64] used a modified DLP printer to fabricate patient-specific biodegradable aortic stents.

Aortic aneurysm and dissections are considered major disease processes affecting the aorta [38]. This disease is often associated with high morbidity and mortality worldwide. The aortic aneurysm is commonly located in the infrarenal abdominal aorta (*Abdominal Aortic Aneurysm; AAA*) and the ascending thoracic aorta (*thoracic aortic aneurysm*). At the organ level, the aneurysm is characterized by a progressive weakening of the aortic wall inducing a local dilation (>50%) of the aorta [167, 168]. Fig. 12 depicts the ascending aortic aneurysm occurring in the ascending portion of the thoracic aorta, a section of the artery close to the heart.

Usually, thoracic aneurysms are treated by a composite aortic graft (Dacron Tube) implant. During the surgical procedure, the aorta's dilated portion is excised and replaced with a prosthetic Dacron tube graft. For the descending thoracic aneurysm, a less invasive approach is proposed. This procedure consists of using a transluminal placed endovascular stent graft [169–171]. Briefly, the stents are made of two components, the metallic structure, which is fabricated from nitinol (nickel-titanium alloy), alloy steel, or 316L stainless steel metal; and the prosthetic conduit, which is made of polytetrafluoroethylene (ePTFE) or polyester fabric [171]. Both components are permanently attached before intra-arterial insertion. Although simple to accomplish, this procedure is not free from post-surgical complications. Ellozy et al. [170] revealed various challenges that have to be addressed to improve endovascular graft efficiency. Among these complications, 38% are device-related, including, but are not limited to, proximal and distal attachment failure, mechanical device failure, and periprocedural death. To reduce these device-related risks, new strategies for stent-graft engineering and fabrications must be elaborated.

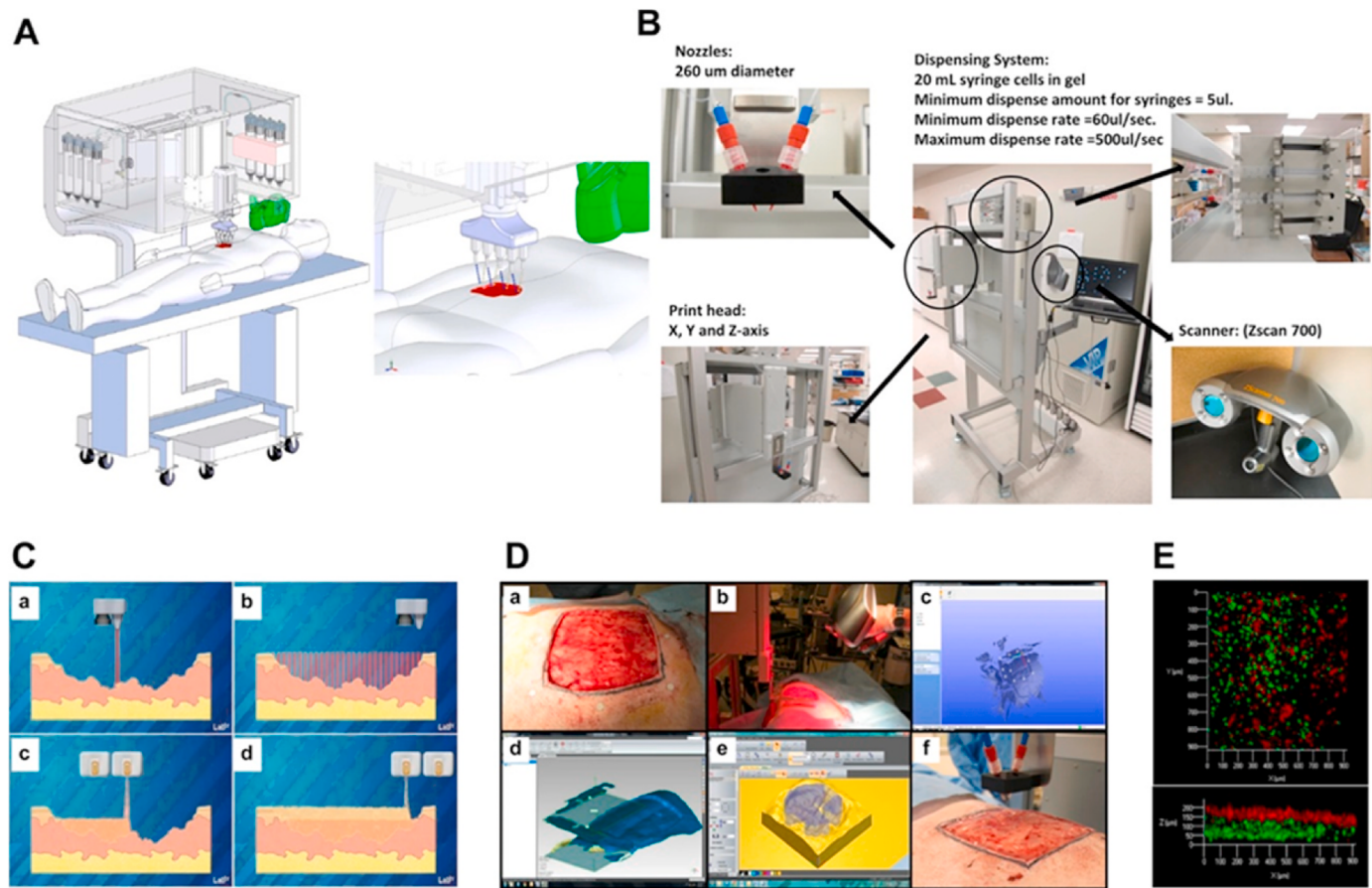


Fig. 11. Skin bioprinter prototype and in situ bioprinting concept.

(A) Schematic demonstrating scale, design, and components of the skin bioprinter. (B) The system's main parts consist of 260 μm diameter nozzles, driven by up to 8 independently dispensing systems connected to a print-head with an XYZ movement system, in addition to the 3D wound scanner. All components are mounted on a frame small enough to be mobile in the operating room. (C) Skin bioprinting concept. Wounds are first scanned to obtain precise information on wound topography, which then guides the print-heads to deposit specified materials and cell types in appropriate locations (Images courtesy of LabTV - National Defense Education Program, Washington, D.C.). (D) An example of a skin bioprinting process, where markers are placed around the wound area used as reference points (a) prior to scanning with a hand-held ZScanner™ Z700 scanner (b). Geometric information obtained via scanning is then inputted in an STL file to orient the scanned images to a standard coordinate system (c). The scanned data with its coordinate system is used to generate the fill volume, and the path points for the nozzle head to travel to print the fill volume (d). Output code is then provided to the custom bioprinter control interface for the nozzle path generation to print fill volume (e,f). (E) This system facilitates the depositing of multiple cell types with high precision and control. The layering of fibroblasts (green) and keratinocytes (red) is shown. Reproduced with permission from Ref. [161]. (For interpretation of the references to colour in this figure legend, the reader is referred to the web version of this article.)

To date, 3DP has been used in the cardiovascular field as a visualization and simulation tool. 3D printing has been used to produce high fidelity patient-customized aortic replicas for planning endovascular stenting in transverse aortic arch hypoplasia [24,36]. Moreover, given the current advances in the 3D bioprinting field demonstrated by intricate vascular network prints [108], future aneurysm therapies might rely on one-demand patient-specific 3D-printed aorta stent [64].

Currently, the number of studies using 3D bioprinting techniques for vascular and valvular tissue engineering is still limited, but studies have been published indicating significant advances in this area. Koc et al. 3D bioprinted a macro-vascular tissue, such as the aorta, directly from the medical images with a bioprinting approach based not on scaffolds or cell-laden hydrogels [172]. Fig. 13 explains the roadmap of the production of the scaffold-free tissue-engineered aorta. After the computer-aided algorithms were developed, mouse embryonic fibroblast (MEF) cell clusters and hydrogel support structures were 3D

bioprinted according to the proposed self-supported method aortic tissue structure. The proposed system can print various cell types such as smooth muscle, endothelial, and fibroblast cells. However, obtaining a sufficient amount of living cells is a challenge, and there is undoubtedly a need for optimized bio-ink preparation for each cell type.

More recently, examples of similar studies in the cardiac field have also been published, with increasing interest in the bioprinting approach without scaffolds. To overcome the limitations of stem cell injection therapies for myocardial infarction treatment, tissue engineering aims to create stable cardiac tissues. The key criteria are the creation of contractile cardiac tissue patches and the vascularization of implanted patches. Yeung et al. 3D bioprinted a biomaterial-free cardiac tissue and evaluated these cardiac patches' *in vivo* regenerative potential [188]. The patches were consisted of cellular spheroids created from coculture of human-induced pluripotent stem cell (iPSC)-derived cardiomyocytes, fibroblasts, and endothelial cells at a ratio of 70:15:15. The bioprinting

Table 5
3D printed multilayered skin substitutes.

Bioinks	Fabrication method	3D Printer	Short Outcomes
Adipose-derived decellularized ECM (dECM) and bovine fibrinogen for hypodermal compartment Skin derived dECM and bovine fibrinogen for dermal compartment Gelatin hydrogel for perfusable and vascularized channel inside the skin tissue model [162] Silk fibroin and gelatin [163]	Extrusion and Inkjet	A self-made extrusion and inkjet-based 3D bioprinter	<ul style="list-style-type: none"> (PCL)-based perfusable well system with the dimensions of 15 mm × 15 mm × 6 mm was also 3D printed to be used for the maturation of the model. The vascular channel was covered by human umbilical vein endothelial cells (HUEVCs) and would supply nutrition and oxygen to encapsulated cells in model The perfusable and vascularized dermis and hypodermis promote physiological cross-talks with epidermal compartment.
Bovine gelatin, very low viscosity alginate and fibrinogen [164]	Extrusion	Self-made deposition system consisting of an extrusion head connected with a pressure controlled pneumatic pump and a direct-write assembly (Fiber Align, Aerotech Inc., Pittsburgh, USA)	<ul style="list-style-type: none"> The enzymatic crosslinking of silk-gelatin using tyrosinase resulted in preservation of structural integrity of the printed constructs until 4 weeks of culture period. Fibroblasts remained embedded in the silk-gelatin bioinks, whereas keratinocytes extensively migrated towards the pores of the bio printed construct by day 14. Although the modulus of native skin was much higher than the 3D bio printed sample, a similar amount of strain was observed at failure. Micro-explants from skin biopsies were used in bioinks and increasing the number of dissociation cycles during mechanical extraction lowered the proliferation of fibroblasts and caused variation between the different sources of biopsy. Keratinocytes cannot proliferate in a 3D environment as an air-liquid interface is required to multiply. Full-thickness wound contraction on the backs of nude mice improved only by approximately 10% compared to the control group (blank) after 4 weeks. No apparent angiogenesis observed <i>in vitro</i>, however <i>in vivo</i> results showed that there was significantly higher number of micro vessels in the dermis the printed skin graft group compared to the control. Viscosity, storage modulus (G'), and loss modulus (G'') of alginate/gelatin composite hydrogels were investigated in terms of printability and 2 wt% alginate/15 wt% gelatin was found to be the optimum concentration. Human amniotic epithelial cells (AECs) differentiated into epithelial cells, while Wharton's jelly derived mesenchymal stem cells (WJMSCs) showed angiogenic potential and fibroblastic phenotype.
Gelatin and sodium alginate composite hydrogels [165]	Extrusion	A custom-made 3D bioprinter consisting of a control system, a mechanism for motion, and feed and nozzle systems	
Alginate and gelatin composite hydrogels [166]	Extrusion	An open-source 3D bioprinter with two syringe heads	

procedure was started with designing the single spheroid layer by using 3D bioprinter software. The 3D bioprinter identified the spheroids' locations in 96-well plates and a robotic arm then used vacuum suction to pick up and transfer and load the cell aggregates individually onto a needle array in exact spatial coordinates to the 3D design. After bioprinting, the cardiac patch was matured for 3 days in the needle array. After printing and culturing, the monolayered 350–400 μm thick cardiac patches were implanted into a rat myocardial infarction model (Fig. 14a). The echocardiography results demonstrated that there is an improvement in cardiac function. Cell retention within implanted patches at 4 weeks post-surgery (Fig. 14 (d–g)) was found to be much higher compared to studies in which more than 85% of cells were lost within 24 h after cell injection therapy.

4. Conclusions & future outlook

Current advances in 3DP technologies and new printing materials engineering have evolved 3DP beyond its initial place and role as a conceptual modeling tool. Today, 3DP has started finding unique and niche applications in a wide range of diverse sectors as a preferred end-product manufacturing technology. The simplicity, flexibility, and agility for complex manufacturing with 3DP have been a significant precursor in this interest boom.

It is necessary to note and highlight the importance that the rise of 3DP popularity has been tightly related to the improvement of printing materials, including biopolymers, thermoplastic polymers, ceramics, metals and composites, in conjunction with integrated innovations in controls, sensing, and automation fields. The biomedical field has

undoubtedly benefited from 3DP technology and materials' evolution, as already seen with tissue engineering products, prosthetics, and implant manufacturing. Moreover, biocompatible materials and dedicated printing devices (bioprinters) have allowed first full organ printing attempts. A challenge in obtaining successful full organ 3D printing

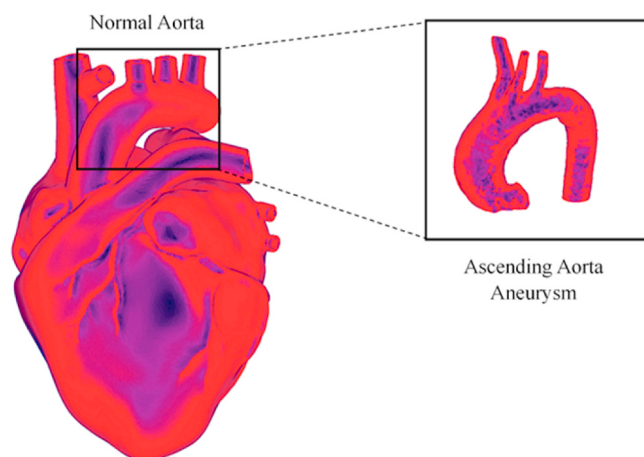


Fig. 12. Thoracic aortic aneurysm. The thoracic aneurysm may target specific thoracic aorta regions, e.g., the ascending part of the aorta (the inset shows the abnormal bulging).

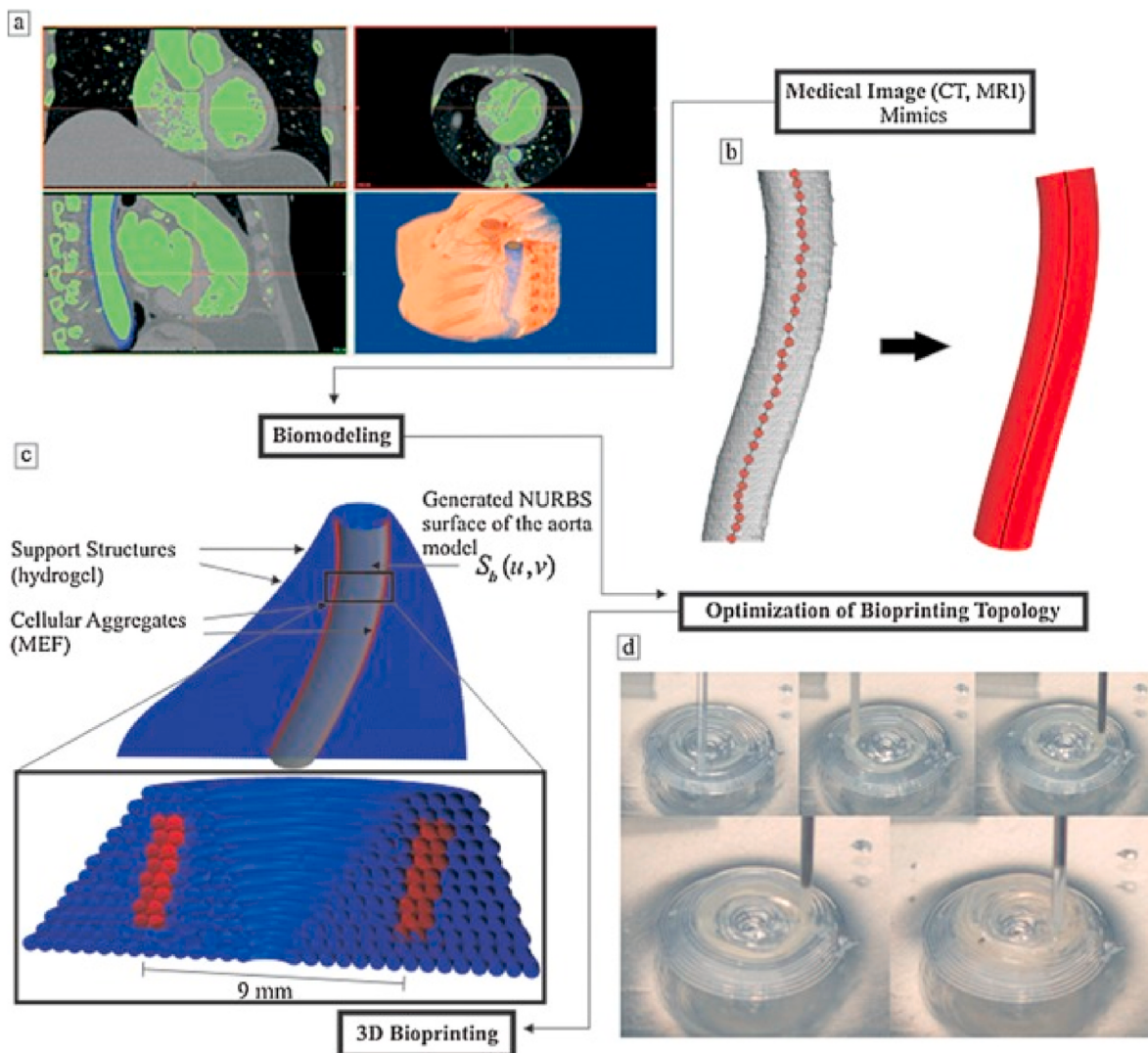


Fig. 13. Roadmap of the proposed methodology.

(a) Segmentation of an aorta from abdominal region based on region growing. (b) The STL (mesh) model of aorta converted to a parametric smooth surface. (c) Representation of the 'Self-Supporting' method, with vessel (grey), cellular aggregates (red) and support structures (blue). (please see the color version) (d) 3D printed MEF cellular aggregates. Reproduced with permission from [172]. (For interpretation of the references to colour in this figure legend, the reader is referred to the web version of this article.)

resides in the complexity of the biological structure that constitutes the said organ. A physiological organ is often composed of an assortment of cells distributed in a given pattern. These cells are perfused with the bloodstream that regularly delivers oxygen and vital nutrient and carries CO_2 and cellular waste to maintain viability. Accordingly, the challenging aspect of full organ bioprinting would be to print various cell types with intricate perfusion systems simultaneously. In addition, currently available bioreactors fail to satisfy the need for adequately simulating cellular conditions to expand large cell populations *in vitro*.

One of the main challenges in today's bioprinting is bio-ink optimization. Obtaining materials that can be processed at high resolutions, preserving the viability of cells at high rates during and after the process, and creating the appropriate cellular environment to direct the desired cell behavior are the requirements that need to be addressed simultaneously. In dense polymers preferred for post-printing shape retention,

important cellular processes such as proliferation, differentiation, and ECM accumulation may be disrupted. While dense networks generally provide the best shape fidelity and 3D printability properties, it has been challenging to balance these advantages and disadvantages in terms of cell viability and function, especially for fragile and sensitive cell types such as pluripotent stem cells that can self-renew indefinitely or differentiate into any cell in the body. Also, porosity, or porous microstructure created by bioinks, is important to allow diffusion of blood for cells to survive until neovascularization is completed.

In addition to the innovations in bioinks, the conventional *in vitro* bioprinting, which relies on the implantation of pre-fabricated constructs, is needed to evolve into *in situ* bioprinting for tissues to be fabricated or repaired directly on the intended anatomical location by using the patient's body as a bioreactor (Fig. 15).

Even though there have been some attempts to *in situ* bioprint

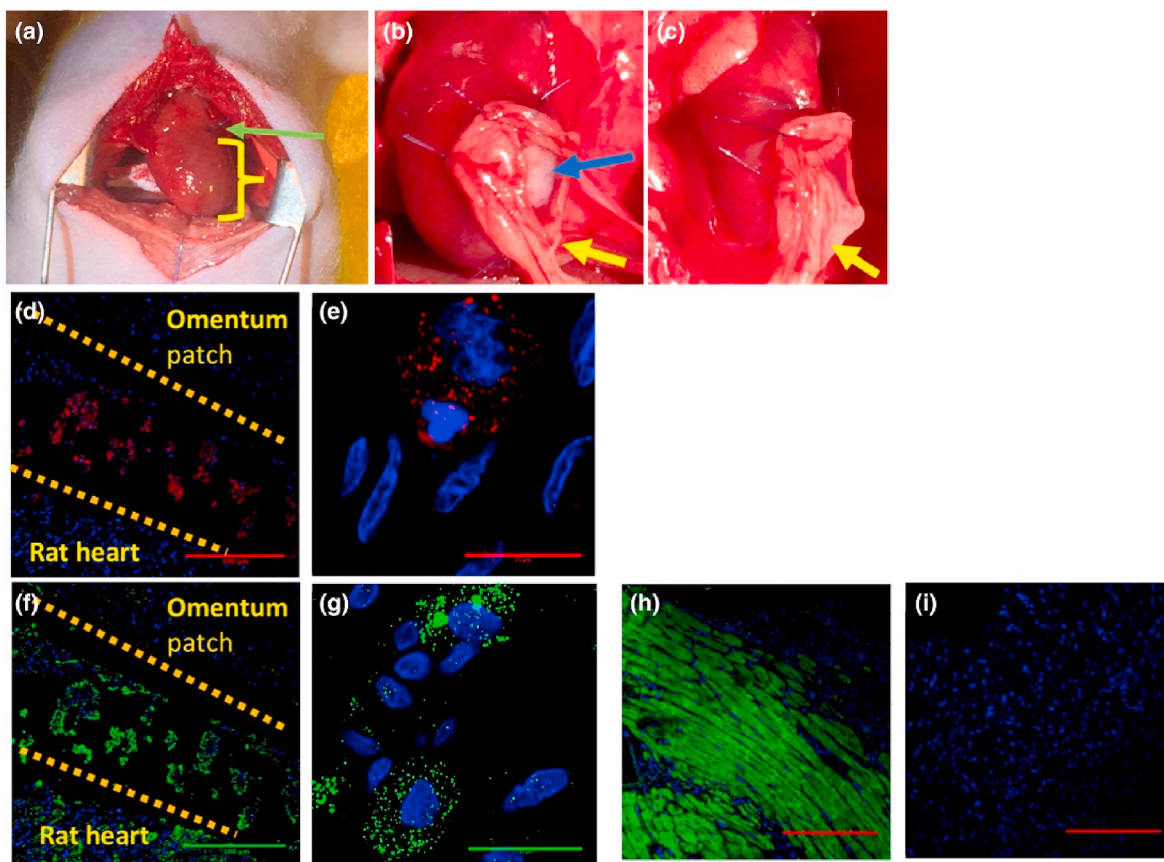


Fig. 14. (a) Occlusion of the distal left anterior descending coronary artery: green arrow, suture and yellow, the infarcted area. (b) Blue arrow, the cardiac patch and yellow arrow, the omentum patch implanted into the experiment group ($n = 6$). (c) The omentum patch implanted in the control group ($n = 6$). (d–g) Evidence of retention of the cells in rat 4 weeks after surgery. Top: the omentum, middle: the patch area, bottom: the rat heart. (d and e) human nuclear antigen (red), DAPI (blue). Red in the patch area: the presence of human nuclear antigen from the stem cell. (d): scale bar = 100 μm , (e): scale bar = 25 μm . (f and g) Troponin T (green), DAPI (blue). Green: the presence of troponin T in both the rat heart and patch area. (f): scale bar = 100 μm , (g): scale bar = 25 μm . (h and i) Positive and negative controls of the troponin T staining, (h): positive control, (i): negative control, scale bar = 100 μm . Reproduced with permission from Ref. [173]. (For interpretation of the references to color in this figure legend, the reader is referred to the Web version of this article.)

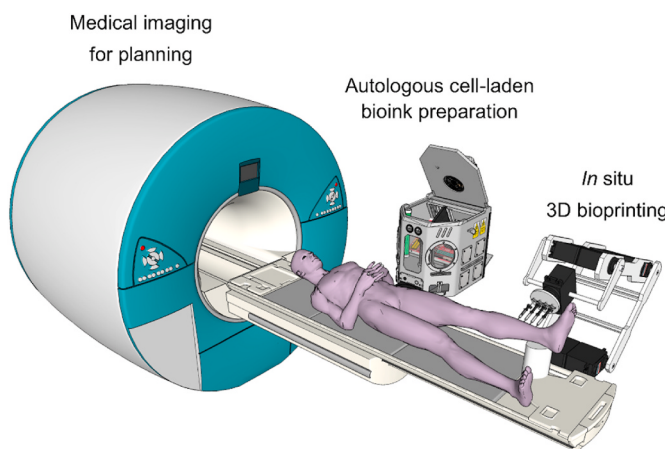


Fig. 15. For the repair of lost/damaged tissues, *in situ* bioprinting utilizes bioinks loaded with the patient-derived cells in a specific anatomical location mostly determined by medical imaging methods.

several tissue types by using robotic arms and handheld devices, serious multidisciplinary innovations are needed to create a simultaneous/sequential operation of medical imaging, patient monitoring, feedback control, and multi-axial bioprinting systems. In addition, the parameters need to be strictly controlled utilizing integrating artificial intelligence

(AI) in the future. Miniaturization and sterilization of bioprinters and nearby devices and making these systems user-friendly for end-user physicians will also be secondary design parameters in the future.

Declaration of competing interest

The authors declare that they have no known competing financial interests or personal relationships that could have appeared to influence the work reported in this paper.

References

- [1] D.F. Viera Rey, J.-P. St-Pierre, Fabrication techniques of tissue engineering scaffolds, in: Handb. Tissue Eng. Scaffolds, Vol. One, Elsevier, 2019, pp. 109–125, <https://doi.org/10.1016/B978-0-08-102563-5.00006-X>.
- [2] ISO, 10993-1:2018, Biological Evaluation of Medical Devices — Part 1: Evaluation and Testing within a Risk Management Process, International Organization for Standardization (ISO), Geneva, 2018.
- [3] M. Kesti, P. Fisch, M. Pensalfini, E. Mazza, M. Zenobi-Wong, Guidelines for standardization of bioprinting: a systematic study of process parameters and their effect on bioprinted structures, *BioNanoMaterials* 17 (2016), <https://doi.org/10.1515/bnm-2016-0004>.
- [4] V. Mironov, The future of medicine: are custom-printed organs on the horizon? *Futurist* 45 (2011) 1.
- [5] A. Su, S.J. Al'Aref, History of 3D printing, in: 3D Print. Appl. Cardiovasc. Med., Elsevier, 2018: pp. 1–10. <https://doi.org/10.1016/B978-0-12-803917-5.00001-8>.
- [6] J. Butt, H. Shirvani, Additive, subtractive, and hybrid manufacturing processes, in: Y. Bar-Cohen (Ed.), *Adv. Manuf. Process. Mater. Struct.*, CRC Press, 2018, pp. 187–218.

- [7] T. Wohlers, T. Gornet, History of Additive Manufacturing, Wohlers Associates, Fort Collins, CO, 2016. Wohlers Report.
- [8] R.R. Jose, M.J. Rodriguez, T.A. Dixon, F.G. Omenetto, D.L. Kaplan, Evolution of bioinks and additive manufacturing technologies for 3D bioprinting, *ACS Biomater. Sci. Eng.* 2 (2016) 1662–1678, <https://doi.org/10.1021/acsbiomaterials.6b00088>.
- [9] P. Kulkarni, D. Dutta, An accurate slicing procedure for layered manufacturing, *Comput. Aided Des.* 28 (1996) 683–697, [https://doi.org/10.1016/0010-4485\(95\)00083-6](https://doi.org/10.1016/0010-4485(95)00083-6).
- [10] P. Mohan Pandey, N. Venkata Reddy, S.G. Dhande, Slicing procedures in layered manufacturing: a review, *Rapid Prototyp. J.* 9 (2003) 274–288, <https://doi.org/10.1108/13552540310502185>.
- [11] ISO/ASTM, 52900-15, Standard Terminology for Additive Manufacturing – General Principles – Terminology, ASTM International, 2015, <https://doi.org/10.1520/F2792-12A>.
- [12] S.C. Ligon, R. Liska, J. Stampfl, M. Gurr, R. Mülhaupt, Polymers for 3D printing and customized additive manufacturing, *Chem. Rev.* 117 (2017) 10212–10290, <https://doi.org/10.1021/acs.chemrev.7b00074>.
- [13] H.S. Ramathan, C.K. Chua, K.F. Leong, K.D. Shah, Melt flow behaviour of poly-e-caprolactone in fused deposition modelling, *J. Mater. Sci. Mater. Med.* 19 (2008) 2541–2550, <https://doi.org/10.1007/s10856-007-3203-6>.
- [14] S. Rangarajan, G. Qi, N. Venkataraman, A. Safari, S.C. Danforth, Powder processing, rheology, and mechanical properties of feedstock for fused deposition of Si3N4 ceramics, *J. Am. Ceram. Soc.* 83 (2004) 1663–1669, <https://doi.org/10.1111/j.1515-2916.2000.tb01446.x>.
- [15] M. Allahverdi, S.C. Danforth, M. Jafari, A. Safari, Processing of advanced electroceramic components by fused deposition technique, *J. Eur. Ceram. Soc.* 21 (2001) 1485–1490, [https://doi.org/10.1016/S0955-2219\(01\)00047-4](https://doi.org/10.1016/S0955-2219(01)00047-4).
- [16] W. Sun, D.J. Dcosta, F. Lin, T. El-Raghy, Freeform fabrication of Ti3SiC2 powder-based structures, *J. Mater. Process. Technol.* 127 (2002) 343–351, [https://doi.org/10.1016/S0924-0136\(02\)00284-4](https://doi.org/10.1016/S0924-0136(02)00284-4).
- [17] M.C. Leu, S. Pattnaik, G.E. Hilmas, Optimization of selective laser sintering process for fabrication of zirconium diboride parts, *Proc 21st Annu. Int Solid Free. Fabr. Symp.* (2010) 493–503.
- [18] M. Niinomi, T. Narushima, M. Nakai (Eds.), *Advances in Metallic Biomaterials: Tissues, Materials and Biological Reactions*, Springer, Heidelberg New York Dordrecht, 2015.
- [19] B.C. Gross, J.L. Erkal, S.Y. Lockwood, C. Chen, D.M. Spence, Evaluation of 3D printing and its potential impact on biotechnology and the chemical sciences, *Anal. Chem.* 86 (2014) 3240–3253, <https://doi.org/10.1021/ac043397r>.
- [20] M. Vukicevic, B. Mosadegh, J.K. Min, S.H. Little, Cardiac 3D printing and its future directions, *JACC Cardiovasc. Imag.* 10 (2017) 171–184, <https://doi.org/10.1016/j.jcmg.2016.12.001>.
- [21] F. Kruijatz, A. Lode, J. Seidel, T. Bley, M. Gelinsky, J. Steingroewer, Additive Biotech—chances, challenges, and recent applications of additive manufacturing technologies in biotechnology, *N. Biotech.* 39 (2017) 222–231, <https://doi.org/10.1016/j.nbt.2017.09.001>.
- [22] M. Suzuki, Y. Ogawa, A. Kawano, A. Hagiwara, H. Yamaguchi, H. Ono, Rapid prototyping of temporal bone for surgical training and medical education, *Acta Otolaryngol. (Stockh.)* 124 (2004) 400–402, <https://doi.org/10.1080/00016480410016478>.
- [23] F. Mahmood, K. Owais, M. Montalegre-Gallegos, R. Matyal, P. Panzica, A. Maslow, K. Khabbaz, Echocardiography derived three-dimensional printing of normal and abnormal mitral annuli, *Ann. Card Anaesth.* 17 (2014) 279, <https://doi.org/10.4103/0971-9784.142062>.
- [24] I. Valverde, G. Gomez, J.F. Coserria, C. Suarez-Mejias, S. Uribe, J. Sotelo, M. N. Velasco, J. Santos De Soto, A.-R. Hosseinpour, T. Gomez-Cia, 3D printed models for planning endovascular stenting in transverse aortic arch hypoplasia: 3D Cardiovascular Model Simulation, *Cathet. Cardiovasc. Interv.* 85 (2015) 1006–1012, <https://doi.org/10.1002/ccd.25810>.
- [25] I. Valverde, G. Gomez, A. Gonzalez, C. Suarez-Mejias, A. Adsuar, J.F. Coserria, S. Uribe, T. Gomez-Cia, A.R. Hosseinpour, Three-dimensional patient-specific cardiac model for surgical planning in Nikaidoh procedure, *Cardiol. Young* 25 (2015) 698–704, <https://doi.org/10.1017/S1047951114000742>.
- [26] H. Seitz, W. Rieder, S. Irsen, B. Leukers, C. Tille, Three-dimensional printing of porous ceramic scaffolds for bone tissue engineering, *J. Biomed. Mater. Res. B Appl. Biomater.* 74B (2005) 782–788, <https://doi.org/10.1002/jbm.b.30291>.
- [27] A. Curodeau, E. Sachs, S. Calderise, Design and fabrication of cast orthopedic implants with freeform surface textures from 3-D printed ceramic shell, *J. Biomed. Mater. Res.* 53 (2002) 525–535, [https://doi.org/10.1002/1097-4636\(200009\)53:5<525::AID-JBMR12>3.0.CO;2-1](https://doi.org/10.1002/1097-4636(200009)53:5<525::AID-JBMR12>3.0.CO;2-1).
- [28] B. Duan, M. Wang, W.Y. Zhou, W.L. Cheung, Z.Y. Li, W.W. Lu, Three-dimensional nanocomposite scaffolds fabricated via selective laser sintering for bone tissue engineering, *Acta Biomater.* 6 (2010) 4495–4505, <https://doi.org/10.1016/j.actbio.2010.06.024>.
- [29] R.L. Simpson, F.E. Wiria, A.A. Amis, C.K. Chua, K.F. Leong, U.N. Hansen, M. Chandrasekaran, M.W. Lee, Development of a 95/5 poly(L-lactide-co-glycolide)/hydroxyapatite and β -tricalcium phosphate scaffold as bone replacement material via selective laser sintering, *J. Biomed. Mater. Res. B Appl. Biomater.* 84B (2008) 17–25, <https://doi.org/10.1002/jbm.b.30839>.
- [30] W.Y. Zhou, S.H. Lee, M. Wang, W.L. Cheung, W.Y. Ip, Selective laser sintering of porous tissue engineering scaffolds from poly(l-lactide)/carbonated hydroxyapatite nanocomposite microspheres, *J. Mater. Sci. Mater. Med.* 19 (2008) 2535–2540, <https://doi.org/10.1007/s10856-007-3089-3>.
- [31] K.-S. Hwang, J.-W. Choi, J.-H. Kim, H. Chung, S. Jin, J.-H. Shim, W.-S. Yun, C.-M. Jeong, J.-B. Huh, Comparative efficacies of collagen-based 3D printed PCL/PLGA/ β -TCP composite block bone grafts and biphasic calcium phosphate bone substitute for bone regeneration, *Materials* 10 (2017) 421, <https://doi.org/10.3390/ma10040421>.
- [32] B. Stevens, Y. Yang, A. Mohandas, B. Stucker, K.T. Nguyen, A review of materials, fabrication methods, and strategies used to enhance bone regeneration in engineered bone tissues, *J. Biomed. Mater. Res. B Appl. Biomater.* 85B (2008) 573–582, <https://doi.org/10.1002/jbm.b.30962>.
- [33] K.-R. Dai, M.-N. Yan, Z.-A. Zhu, Y.-H. Sun, Computer-aided custom-made hemipelvis prosthesis used in extensive pelvic lesions, *J. Arthroplasty* 22 (2007) 981–986, <https://doi.org/10.1016/j.arth.2007.05.002>.
- [34] M.-Y. Lee, C.-C. Chang, Y.C. Ku, New layer-based imaging and rapid prototyping techniques for computer-aided design and manufacture of custom dental restoration, *J. Med. Eng. Technol.* 32 (2008) 83–90, <https://doi.org/10.1080/03091900600836642>.
- [35] P.S. D'Urso, D.J. Effeney, W.J. Earwaker, T.M. Barker, M.J. Redmond, R. G. Thompson, F.H. Tomlinson, Custom cranioplasty using stereolithography and acrylic, *Br. J. Plast. Surg.* 53 (2000) 200–204, <https://doi.org/10.1054/bjps.1999.3268>.
- [36] D. Yuan, H. Luo, H. Yang, B. Huang, J. Zhu, J. Zhao, Precise treatment of aortic aneurysm by three-dimensional printing and simulation before endovascular intervention, *Sci. Rep.* 7 (2017) 795, <https://doi.org/10.1038/s41598-017-00644-4>.
- [37] A. Müller, K.G. Krishnan, E. Uhl, G. Mast, The application of rapid prototyping techniques in cranial reconstruction and preoperative planning in neurosurgery: *J. Craniofac. Surg.* 14 (2003) 899–914, <https://doi.org/10.1097/00001665-200311000-00014>.
- [38] J. Faber, P.M. Berto, M. Quaresma, Rapid prototyping as a tool for diagnosis and treatment planning for maxillary canine impaction, *Am. J. Orthod. Dentofacial Orthop.* 129 (2006) 583–589, <https://doi.org/10.1016/j.ajodo.2005.12.015>.
- [39] T.M. Binder, D. Moertl, G. Mundigler, G. Rehak, M. Franke, G. Delle-Karth, W. Mohl, H. Baumgartner, G. Maurer, Stereolithographic biomodeling to create tangible hard copies of cardiac structures from echocardiographic data, *J. Am. Coll. Cardiol.* 35 (2000) 230–237, [https://doi.org/10.1016/S0735-1097\(99\)00498-2](https://doi.org/10.1016/S0735-1097(99)00498-2).
- [40] M.S. Kim, A.R. Hansgen, J.D. Carroll, Use of rapid prototyping in the care of patients with structural heart disease, *Trends Cardiovasc. Med.* 18 (2008) 210–216, <https://doi.org/10.1016/j.tcm.2008.11.001>.
- [41] K. Knox, C.W. Kerber, S.A. Singel, M.J. Bailey, S.G. Imbesi, Rapid prototyping to create vascular replicas from CT scan data: making tools to teach, rehearse, and choose treatment strategies, *Catheter. Cardiovasc. Interv.* 65 (2005) 47–53, <https://doi.org/10.1002/ccd.20333>.
- [42] M.S. Kim, A.R. Hansgen, O. Wink, R.A. Quaife, J.D. Carroll, Rapid prototyping: a new tool in understanding and treating structural heart disease, *Circulation* 117 (2008) 2388–2394, <https://doi.org/10.1161/CIRCULATIONAHA.107.740977>.
- [43] R. Landers, R. Mülhaupt, Desktop manufacturing of complex objects, prototypes and biomedical scaffolds by means of computer-assisted design combined with computer-guided 3D plotting of polymers and reactive oligomers, *Macromol. Mater. Eng.* 282 (2000) 5, [https://doi.org/10.1002/1439-2054\(20001001\)282:1<17:AID-MAME17>3.0.CO;2-8](https://doi.org/10.1002/1439-2054(20001001)282:1<17:AID-MAME17>3.0.CO;2-8).
- [44] S. Wüst, M.E. Godla, R. Müller, S. Hofmann, Tunable hydrogel composite with two-step processing in combination with innovative hardware upgrade for cell-based three-dimensional bioprinting, *Acta Biomater.* 10 (2014) 630–640, <https://doi.org/10.1016/j.actbio.2013.10.016>.
- [45] R. Landers, A. Pfister, U. Hübner, H. John, R. Schmelzeisen, R. Mülhaupt, Fabrication of soft tissue engineering scaffolds by means of rapid prototyping techniques, *J. Mater. Sci.* 37 (2002) 3107–3116, <https://doi.org/10.1023/A:1016189724389>.
- [46] S. Ahn, H. Lee, E.J. Lee, G. Kim, A direct cell printing supplemented with low-temperature processing method for obtaining highly porous three-dimensional cell-laden scaffolds, *J. Mater. Chem. B* 2 (2014) 2773, <https://doi.org/10.1039/c4tb00139g>.
- [47] B. Derby, Printing and prototyping of tissues and scaffolds, *Science* 338 (2012) 921–926, <https://doi.org/10.1126/science.1226340>.
- [48] D. Maragianis, M.S. Jackson, S.R. Igo, R.C. Schutt, P. Connell, J. Grande-Allen, C.M. Barker, S.M. Chang, M.J. Reardon, W.A. Zoghbi, S.H. Little, Replicating patient-specific severe aortic valve stenosis with functional 3D modeling, *Circ. Cardiovasc. Imag.* 8 (2015), <https://doi.org/10.1161/CIRCIMAGING.115.003626>.
- [49] N.P. Macdonald, F. Zhu, C.J. Hall, J. Reboud, P.S. Crosier, E.E. Patton, D. Wlodkowic, J.M. Cooper, Assessment of biocompatibility of 3D printed photopolymers using zebrafish embryo toxicity assays, *Lab Chip* 16 (2016) 291–297, <https://doi.org/10.1039/CSLC01374G>.
- [50] M. Touri, F. Moztarzadeh, N.A.A. Osman, M.M. Dehghan, M. Mozafari, 3D-printed biphasic calcium phosphate scaffolds coated with an oxygen generating system for enhancing engineered tissue survival, *Mater. Sci. Eng. C* 84 (2018) 236–242, <https://doi.org/10.1016/j.msec.2017.11.037>.
- [51] L. Elomaa, S. Teixeira, R. Hakala, H. Korhonen, D.W. Grijpma, J.V. Seppälä, Preparation of poly(e-caprolactone)-based tissue engineering scaffolds by stereolithography, *Acta Biomater.* 7 (2011) 3850–3856, <https://doi.org/10.1016/j.actbio.2011.06.039>.
- [52] A.A. Mäkitie, J. Korpela, L. Elomaa, M. Reivonen, A. Kokkari, M. Malin, H. Korhonen, X. Wang, J. Salo, E. Siilvo, M. Salmi, J. Partanen, K.-S. Paloheimo, J. Tuomi, T. Närhi, J. Seppälä, Novel additive manufactured scaffolds for tissue engineered trachea research, *Acta Otolaryngol. (Stockh.)* 133 (2013) 412–417, <https://doi.org/10.3109/00016489.2012.761725>.

- [53] S.B. Lowe, V.T.G. Tan, A.H. Soeriyadi, T.P. Davis, J.J. Gooding, Synthesis and high-throughput processing of polymeric hydrogels for 3D cell culture, *Bioconjugate Chem.* 25 (2014) 1581–1601, <https://doi.org/10.1021/bc500310v>.
- [54] J.A. Barron, B.R. Ringeisen, H. Kim, B.J. Spargo, D.B. Chrisey, Application of laser printing to mammalian cells, *Thin Solid Films* (2004) 453–454, <https://doi.org/10.1016/j.tsf.2003.11.161>, 383–387.
- [55] C.M. Smith, A.L. Stone, R.L. Parkhill, R.L. Stewart, M.W. Simpkins, A. M. Kachurin, W.L. Warren, S.K. Williams, Three-dimensional BioAssembly tool for generating viable tissue-engineered constructs, *Tissue Eng.* 10 (2004) 1566–1576, <https://doi.org/10.1089/ten.2004.10.1566>.
- [56] T. Xu, J. Olson, W. Zhao, A. Atala, J.-M. Zhu, J.J. Yoo, Characterization of cell constructs generated with inkjet printing technology using *in vivo* magnetic resonance imaging, *J. Manuf. Sci. Eng.* 130 (2008), 021013, <https://doi.org/10.1115/1.2902857>.
- [57] T. Xu, H. Kincaid, A. Atala, J.J. Yoo, High-throughput production of single-cell microparticles using an inkjet printing technology, *J. Manuf. Sci. Eng.* 130 (2008), 021017, <https://doi.org/10.1115/1.2903064>.
- [58] S.V. Murphy, A. Atala, 3D bioprinting of tissues and organs, *Nat. Biotechnol.* 32 (2014) 773–785, <https://doi.org/10.1038/nbt.2958>.
- [59] B. Guillotin, A. Souquet, S. Catros, M. Duocastella, B. Pippenger, S. Bellance, R. Bareille, M. Rémy, L. Bordenave, J. Amédée, F. Guillemot, Laser assisted bioprinting of engineered tissue with high cell density and microscale organization, *Biomaterials* 31 (2010) 7250–7256, <https://doi.org/10.1016/j.biomaterials.2010.05.055>.
- [60] K. Iwami, T. Noda, K. Ishida, K. Morishima, M. Nakamura, N. Umeda, Bio rapid prototyping by extruding/aspirating/refilling thermoreversible hydrogel, *Biofabrication* 2 (2010), 014108, <https://doi.org/10.1088/1758-5082/2/1/014108>.
- [61] T. Xu, W. Zhao, J.-M. Zhu, M.Z. Albanna, J.J. Yoo, A. Atala, Complex heterogeneous tissue constructs containing multiple cell types prepared by inkjet printing technology, *Biomaterials* 34 (2013) 130–139, <https://doi.org/10.1016/j.biomaterials.2012.09.035>.
- [62] T. Xu, J. Jin, C. Gregory, J.J. Hickman, T. Boland, Inkjet printing of viable mammalian cells, *Biomaterials* 26 (2005) 93–99, <https://doi.org/10.1016/j.biomaterials.2004.04.011>.
- [63] U. Jammalamadaka, K. Tappa, Recent advances in biomaterials for 3D printing and tissue engineering, *J. Funct. Biomater.* 9 (2018) 22, <https://doi.org/10.3390/jfb9010022>.
- [64] H.O.T. Ware, A.C. Farsheed, B. Akar, C. Duan, X. Chen, G. Ameer, C. Sun, High-speed on-demand 3D printed bioresorbable vascular scaffolds, *Mater. Today Chem.* 7 (2018) 25–34, <https://doi.org/10.1016/j.mtchem.2017.10.002>.
- [65] W. Wu, Q. Zheng, X. Guo, J. Sun, Y. Liu, A programmed release multi-drug implant fabricated by three-dimensional printing technology for bone tuberculosis therapy, *Biomed. Mater.* 4 (2009), 065005, <https://doi.org/10.1088/1748-6041/4/6/065005>.
- [66] K.F. Leong, F.E. Wiria, C.K. Chua, S.H. Li, Characterization of a poly-epsilon-caprolactone polymeric drug delivery device built by selective laser sintering, *Bio Med. Mater. Eng.* 17 (2007) 147–157.
- [67] J. Holländer, N. Genina, H. Jukarainen, M. Khajeheian, A. Rosling, E. Mäkilä, N. Sandler, Three-dimensional printed PCL-based implantable prototypes of medical devices for controlled drug delivery, *J. Pharm. Sci.* 105 (2016) 2665–2676, <https://doi.org/10.1016/j.xphs.2015.12.012>.
- [68] N. Genina, J. Holländer, H. Jukarainen, E. Mäkilä, J. Salonen, N. Sandler, Ethylene vinyl acetate (EVA) as a new drug carrier for 3D printed medical drug delivery devices, *Eur. J. Pharmaceut. Sci.* 90 (2016) 53–63, <https://doi.org/10.1016/j.ejps.2015.11.005>.
- [69] J. Skowyra, K. Pietrzak, M.A. Alhnan, Fabrication of extended-release patient-tailored prednisolone tablets via fused deposition modelling (FDM) 3D printing, *Eur. J. Pharmaceut. Sci.* 68 (2015) 11–17, <https://doi.org/10.1016/j.ejps.2014.11.009>.
- [70] B.M. Wu, S.W. Borland, R.A. Giordano, L.G. Cima, E.M. Sachs, M.J. Cima, Solid free-form fabrication of drug delivery devices, *J. Contr. Release* 40 (1996) 77–87, [https://doi.org/10.1016/0168-3659\(95\)00173-5](https://doi.org/10.1016/0168-3659(95)00173-5).
- [71] M. Palo, J. Holländer, J. Suominen, J. Ylirusi, N. Sandler, 3D printed drug delivery devices: perspectives and technical challenges, *Expert Rev. Med. Dev.* 14 (2017) 685–696, <https://doi.org/10.1080/17434440.2017.1363647>.
- [72] V. Mironov, N. Reis, B. Derby, Review: bioprinting: A beginning, *Tissue Eng.* 12 (2006) 631–634, <https://doi.org/10.1089/ten.2006.12.631>.
- [73] P.J. Bártolo, I. Gibson, History of stereolithographic processes, in: P.J. Bártolo (Ed.), *Stereolithography*, Springer US, Boston, MA, 2011, pp. 37–56, https://doi.org/10.1007/978-0-387-92904-0_2.
- [74] F.P.W. Melchels, J. Feijen, D.W. Grijpma, A review on stereolithography and its applications in biomedical engineering, *Biomaterials* 31 (2010) 6121–6130, <https://doi.org/10.1016/j.biomaterials.2010.04.050>.
- [75] R.A. Giordano, B.M. Wu, S.W. Borland, L.G. Cima, E.M. Sachs, M.J. Cima, Mechanical properties of dense polylactic acid structures fabricated by three dimensional printing, *J. Biomater. Sci. Polym. Ed.* 8 (1997) 63–75, <https://doi.org/10.1163/156856297X00588>.
- [76] B. Dhariwala, E. Hunt, T. Boland, Rapid prototyping of tissue-engineering constructs, using photopolymerizable hydrogels and stereolithography, *Tissue Eng.* 10 (2004) 1316–1322, <https://doi.org/10.1089/ten.2004.10.1316>.
- [77] J.M. Lee, S.L. Sing, M. Zhou, W.Y. Yeong, 3D bioprinting processes: a perspective on classification and terminology, *Int. J. Bioprinting.* 4 (2018), <https://doi.org/10.18063/jjb.v4i2.151>.
- [78] H. Lin, D. Zhang, P.G. Alexander, G. Yang, J. Tan, A.W.-M. Cheng, R.S. Tuan, Application of visible light-based projection stereolithography for live cell-scaffold fabrication with designed architecture, *Biomaterials* 34 (2013) 331–339, <https://doi.org/10.1016/j.biomaterials.2012.09.048>.
- [79] Z. Wang, R. Abdulla, B. Parker, R. Samanipour, S. Ghosh, K. Kim, A simple and high-resolution stereolithography-based 3D bioprinting system using visible light crosslinkable bioinks, *Biofabrication* 7 (2015), 045009, <https://doi.org/10.1088/1758-5090/7/4/045009>.
- [80] S. Monneret, V. Loubere, S. Corbel, in: B. Courtois, S.B. Crary, W. Ehrfeld, H. Fujita, J.M. Karam, K.W. Markus (Eds.), *Microstereolithography Using a Dynamic Mask Generator and a Noncoherent Visible Light Source*, 1999, p. 553, <https://doi.org/10.1117/12.341246>. Paris, France.
- [81] C. Sun, N. Fang, D.M. Wu, X. Zhang, Projection micro-stereolithography using digital micro-mirror dynamic mask, *Sens. Actuators Phys.* 121 (2005) 113–120, <https://doi.org/10.1016/j.sna.2004.12.011>.
- [82] R. Xie, D. Li, S. Chao, An inexpensive stereolithography technology with high power UV-LED light, *Rapid Prototyp. J.* 17 (2011) 441–450, <https://doi.org/10.1108/1355241111814170>.
- [83] S.H. Kim, Y.K. Yeon, J.M. Lee, J.R. Chao, Y.J. Lee, Y.B. Seo, MdT. Sultan, O.J. Lee, J.S. Lee, S. Yoon, I.-S. Hong, G. Khang, S.J. Lee, J.J. Yoo, C.H. Park, Precisely printable and biocompatible silk fibroin bioink for digital light processing 3D printing, *Nat. Commun.* 9 (2018) 1620, <https://doi.org/10.1038/s41467-018-03759-y>.
- [84] R. Felzmann, S. Gruber, G. Mitteramskogler, P. Tesavibul, A.R. Boccaccini, R. Liska, J. Stampfl, Lithography-based additive manufacturing of cellular ceramic structures, *Adv. Eng. Mater.* 14 (2012) 1052–1058, <https://doi.org/10.1002/adem.201200010>.
- [85] A. Bagheri Saed, A.H. Behravesh, S. Hasannia, S.A. Alavinasab Ardebili, B. Akhondi, M. Pourghayoumi, Functionalized poly l-lactic acid synthesis and optimization of process parameters for 3D printing of porous scaffolds via digital light processing (DLP) method, *J. Manuf. Process.* 56 (2020) 550–561, <https://doi.org/10.1016/j.jmapro.2020.04.076>.
- [86] J.Z. Manapat, Q. Chen, P. Ye, R.C. Advincula, 3D printing of polymer nanocomposites via stereolithography, *Macromol. Mater. Eng.* 302 (2017) 1600553, <https://doi.org/10.1002/mame.201600553>.
- [87] C.M.B. Ho, S.H. Ng, K.H.H. Li, Y.-J. Yoon, 3D printed microfluidics for biological applications, *Lab Chip* 15 (2015) 3627–3637, <https://doi.org/10.1039/C5LC00685F>.
- [88] A. Ovsianikov, S. Mühlender, J. Torgersen, Z. Li, X.-H. Qin, S. Van Vlierbergh, P. Dubrule, W. Holnthoner, H. Redl, R. Liska, J. Stampfl, Laser photofabrication of cell-containing hydrogel constructs, *Langmuir* 30 (2014) 3787–3794, <https://doi.org/10.1021/la402346z>.
- [89] H. Yu, J. Liu, Y. Li, Y. Zhao, F. Jin, X.-Z. Dong, Z.-S. Zhao, X.-M. Duan, M.-L. Zheng, Biocompatible three-dimensional hydrogel cell scaffold fabricated by sodium hyaluronate and chitosan assisted two-photon polymerization, *ACS Appl. Bio Mater.* 2 (2019) 3077–3083, <https://doi.org/10.1021/acsabm.9b00384>.
- [90] S.S. Crump, A.E.-P.D. Muir, Apparatus and method for creating three-dimensional objects 5 (121) (1992) 329.
- [91] W. Wu, P. Geng, G. Li, D. Zhao, H. Zhang, J. Zhao, Influence of layer thickness and raster angle on the mechanical properties of 3D-printed PEEK and a comparative mechanical study between PEEK and ABS, *Materials* 8 (2015) 5834–5846, <https://doi.org/10.3390/ma8095271>.
- [92] V.K. Tiwary, P. Arunkumar, A.S. Deshpande, N. Rangaswamy, Surface enhancement of FDM patterns to be used in rapid investment casting for making medical implants, *Rapid Prototyp. J.* 25 (2019) 904–914.
- [93] J.S. Chohan, R. Singh, Enhancing dimensional accuracy of FDM based biomedical implant replicas by statistically controlled vapor smoothing process, *Prog. Addit. Manuf.* 1 (2016) 105–113, <https://doi.org/10.1007/s40964-016-0009-4>.
- [94] M.B. Burn, A. Ta, G.R. Gogola, Three-dimensional printing of prosthetic hands for children, *J. Hand Surg.* 41 (2016) e103–e109, <https://doi.org/10.1016/j.jhsa.2016.02.008>.
- [95] J.P. Bustillo, R. Tumlos, R.Z. Remoto, Intensity modulated radiotherapy (IMRT) phantom fabrication using fused deposition modeling (FDM) 3D printing technique, in: L. Lhotska, L. Sukupova, I. Lacković, G.S. Ibott (Eds.), *World Congr. Med. Phys. Biomed. Eng.* 2018, Springer Singapore, Singapore, 2019, pp. 509–515, https://doi.org/10.1007/978-981-10-9023-3_92.
- [96] E.J. McCullough, V.K. Yadavalli, Surface modification of fused deposition modeling ABS to enable rapid prototyping of biomedical microdevices, *J. Mater. Process. Technol.* 213 (2013) 947–954, <https://doi.org/10.1016/j.jmatprotec.2012.12.015>.
- [97] J.F. Christ, N. Aliheidari, A. Ameli, P. Pötschke, 3D printed highly elastic strain sensors of multiwalled carbon nanotube/thermoplastic polyurethane nanocomposites, *Mater. Des.* 131 (2017) 394–401, <https://doi.org/10.1016/j.matedes.2017.06.011>.
- [98] Q. Chen, J.D. Mangadlo, J. Wallat, A. De Leon, J.K. Pokorski, R.C. Advincula, 3D printing biocompatible polyurethane/poly(lactic acid)/graphene oxide nanocomposites: anisotropic properties, *ACS Appl. Mater. Interfaces* 9 (2017) 4015–4023, <https://doi.org/10.1021/acsami.6b11793>.
- [99] X. Wang, Y. Yan, Y. Pan, Z. Xiong, H. Liu, J. Cheng, F. Liu, F. Lin, R. Wu, R. Zhang, Q. Lu, Generation of three-dimensional hepatocyte/gelatin structures with rapid prototyping system, *Tissue Eng.* 12 (2006) 83–90, <https://doi.org/10.1089/tten.2006.12.83>.
- [100] W. Liu, Z. Zhong, N. Hu, Y. Zhou, L. Maggio, A.K. Miri, A. Fragasso, X. Jin, A. Khademhosseini, Y.S. Zhang, Coaxial extrusion bioprinting of 3D microfibrous constructs with cell-favorable gelatin methacryloyl microenvironments, *Biofabrication* 10 (2018), 024102, <https://doi.org/10.1088/1758-5090/aa9d44>.
- [101] H. Wijshoff, The dynamics of the piezo inkjet printhead operation*, *Phys. Rep.* 491 (2010) 77–177, <https://doi.org/10.1016/j.physrep.2010.03.003>.

- [102] B.C. Te, J.T. Wigand, Method and Apparatus for Fabricating Three Dimensional Models, 2015, 2015/0147421 A1.
- [103] W.E. Masters, Computer Automated Manufacturing Process and System, 4, 1987, 665,492.
- [104] M. Yamane, T. Kawaguchi, Apparatus For Forming Three-Dimensional Article, 5, 1992, 140,937.
- [105] S.M. Penn, System, method, and process For Making Three-Dimensional Objects, 5, 1993, 260,009.
- [106] M. Salmi, K.-S. Paloheimo, J. Tuomi, J. Wolff, A. Mäkitie, Accuracy of medical models made by additive manufacturing (rapid manufacturing), *J. Cranio-Maxillo-Fac. Surg.* 41 (2013) 603–609, <https://doi.org/10.1016/j.jcm.2012.11.041>.
- [107] S. Minocchieri, J.M. Burren, M.A. Bachmann, G. Stern, J. Wildhaber, S. Buob, R. Schindel, R. Kraemer, U.P. Frey, M. Nelle, Development of the premature infant nose throat-model (PrINT-Model)—an upper airway replica of a premature neonate for the study of aerosol delivery, *Pediatr. Res.* 64 (2008) 141–146, <https://doi.org/10.1203/R.Db013e318175dcfa>.
- [108] A.D. Castiaux, C.W. Pinger, E.A. Hayter, M.E. Bunn, R.S. Martin, D.M. Spence, PolyJet 3D-printed enclosed microfluidic channels without photocurable supports, *Anal. Chem.* 91 (2019) 6910–6917, <https://doi.org/10.1021/acs.analchem.9b01302>.
- [109] T. Boland, W.C. Wilson, T. Xu, Inkjet Printing of Viable Cells, 7, 2006, 051,654 B2.
- [110] H. Cui, M. Nowicki, J.P. Fisher, L.G. Zhang, 3D bioprinting for organ regeneration, *Adv. Healthc. Mater.* 6 (2017), <https://doi.org/10.1002/adhm.201601118>.
- [111] B. Zhang, Y. Luo, L. Ma, L. Gao, Y. Li, Q. Xue, H. Yang, Z. Cui, 3D bioprinting: an emerging technology full of opportunities and challenges, *Bio-Des. Manuf.* 1 (2018) 2–13, <https://doi.org/10.1007/s42242-018-0004-3>.
- [112] D.J. Odde, M.J. Renn, Laser-guided direct writing for applications in biotechnology, *Trends Biotechnol.* 17 (1999) 385–389, [https://doi.org/10.1016/S0167-7799\(99\)01355-4](https://doi.org/10.1016/S0167-7799(99)01355-4).
- [113] H.-W. Kang, S.J. Lee, I.K. Ko, C. Kengla, J.J. Yoo, A. Atala, A 3D bioprinting system to produce human-scale tissue constructs with structural integrity, *Nat. Biotechnol.* 34 (2016) 312–319, <https://doi.org/10.1038/nbt.3413>.
- [114] E. Sachs, M. Cima, P. Williams, D. Brancazio, J. Cornie, Three dimensional printing: rapid tooling and prototypes directly from a CAD model, *J. Eng. Ind.* 114 (1992) 481, <https://doi.org/10.1115/1.2900701>.
- [115] E. Mancuso, N. Alharbi, O.A. Bretcanu, M. Marshall, M.A. Birch, A.W. McCaskie, K.W. Dalgarno, Three-dimensional printing of porous load-bearing bioceramic scaffolds, *Proc. Inst. Mech. Eng. [H]*, 231 (2017) 575–585, <https://doi.org/10.1177/0954411916682984>.
- [116] D. Hong, D.-T. Chou, O.I. Velikokhatnyi, A. Roy, B. Lee, I. Swink, I. Issaev, H. A. Kuhn, P.N. Kumta, Binder-jetting 3D printing and alloy development of new biodegradable Fe-Mn-Ca/Mg alloys, *Acta Biomater.* 45 (2016) 375–386, <https://doi.org/10.1016/j.actbio.2016.08.032>.
- [117] D.-T. Chou, D. Wells, D. Hong, B. Lee, H. Kuhn, P.N. Kumta, Novel processing of iron–manganese alloy-based biomaterials by inkjet 3-D printing, *Acta Biomater.* 9 (2013) 8593–8603, <https://doi.org/10.1016/j.actbio.2013.04.016>.
- [118] M.M. Savalani, L. Hao, R.A. Harris, Evaluation of CO₂ and Nd:YAG lasers for the selective laser sintering of HAPEX®, *Proc. Inst. Mech. Eng. Part B J. Eng. Manuf.* 220 (2006) 171–182, <https://doi.org/10.1243/09544050X32986>.
- [119] L. Yuan, S. Ding, C. Wen, Additive manufacturing technology for porous metal implant applications and triple minimal surface structures: a review, *Bioact. Mater.* 4 (2019) 56–70, <https://doi.org/10.1016/j.bioactmat.2018.12.003>.
- [120] H. Galarraga, D.A. Lados, R.R. Dehoff, M.M. Kirka, P. Nandwana, Effects of the microstructure and porosity on properties of Ti-6Al-4V ELI alloy fabricated by electron beam melting (EBM), *Addit. Manuf.* 10 (2016) 47–57, <https://doi.org/10.1016/j.addma.2016.02.003>.
- [121] S. Kumar, Selective laser sintering: a qualitative and objective approach, *JOM* 55 (2003) 43–47, <https://doi.org/10.1007/s11837-003-0175-y>.
- [122] A.K. Ibraheem, B. Derby, P.J. Withers, Thermal and residual stress modelling of the selective laser sintering process, *MRS Proc.* 758 (2002), <https://doi.org/10.1557/PROC-758-LL1.8>. LL1.8.
- [123] B. Liu, L. Zhang, J. Mo, B. Qian, New method of improving parts accuracy by adding heat balance support in selective laser sintering, *J. Zhejiang Univ. - Sci. A*, 10 (2009) 361–369, <https://doi.org/10.1631/jzus.A0820226>.
- [124] M. Yakout, A. Cadamuro, M.A. Elbestawi, S.C. Veldhuis, The selection of process parameters in additive manufacturing for aerospace alloys, *Int. J. Adv. Manuf. Technol.* 92 (2017) 2081–2098, <https://doi.org/10.1007/s00170-017-0280-7>.
- [125] J.T. Rimell, P.M. Marquis, Selective laser sintering of ultra high molecular weight polyethylene for clinical applications, *J. Biomed. Mater. Res.* 53 (2000) 414–420, [https://doi.org/10.1002/1097-4636\(2000\)53:4<414::aid-jbm16>3.0.co;2-m](https://doi.org/10.1002/1097-4636(2000)53:4<414::aid-jbm16>3.0.co;2-m).
- [126] J. Cheng, S. Lao, K. Nguyen, W. Ho, A. Cummings, J. Koo, SLS processing studies of nylon 11 nanocomposites, in: *Proc Int Solid Free. Fabr. Symp.*, 2005, pp. 141–149.
- [127] G.V. Salmoria, J.L. Leite, R.A. Paggi, The microstructural characterization of PA6/PA12 blend specimens fabricated by selective laser sintering, *Polym. Test.* 28 (2009) 746–751, <https://doi.org/10.1016/j.polymertesting.2009.06.010>.
- [128] R.D. Goodridge, C.J. Tuck, R.J.M. Hague, Laser sintering of polyamides and other polymers, *Prog. Mater. Sci.* 57 (2012) 229–267, <https://doi.org/10.1016/j.pmatsci.2011.04.001>.
- [129] W.Y. Zhou, B. Duan, M. Wang, W.L. Cheung, Crystallization kinetics of poly(L-lactide)/carbonated hydroxyapatite nanocomposite microspheres, *J. Appl. Polym. Sci.* 113 (2009) 4100–4115, <https://doi.org/10.1002/app.30527>.
- [130] G. Turnbull, J. Clarke, F. Picard, P. Riches, L. Jia, F. Han, B. Li, W. Shu, 3D bioactive composite scaffolds for bone tissue engineering, *Bioact. Mater.* 3 (2018) 278–314, <https://doi.org/10.1016/j.bioactmat.2017.10.001>.
- [131] A. Pacifici, L. Laino, M. Gargari, F. Guzzo, A. Velandia Luz, A. Polimeni, L. Pacifici, Decellularized hydrogels in bone tissue engineering: a topical review, *Int. J. Med. Sci.* 15 (2018) 492–497, <https://doi.org/10.7150/ijms.22789>.
- [132] N. Ashammakh, O. Kaarela, Three-dimensional bioprinting can help bone, *J. Craniofac. Surg.* 29 (2018) 9–11, <https://doi.org/10.1097/SCS.00000000000004143>.
- [133] L. Zhang, G. Yang, B.N. Johnson, X. Jia, Three-dimensional (3D) printed scaffold and material selection for bone repair, *Acta Biomater.* 84 (2019) 16–33, <https://doi.org/10.1016/j.actbio.2018.11.039>.
- [134] M. Neufurth, X. Wang, S. Wang, R. Steffen, M. Ackermann, N.D. Haep, H. C. Schröder, W.E.G. Müller, 3D printing of hybrid biomaterials for bone tissue engineering: calcium-polyphosphate microparticles encapsulated by polycaprolactone, *Acta Biomater.* 64 (2017) 377–388, <https://doi.org/10.1016/j.actbio.2017.09.031>.
- [135] M.O. Aydogdu, E.T. Oner, N. Eken, G. Erdemir, S.E. Kuruca, E. Yuca, M. S. Bostan, M.S. Eroglu, F. Ikram, M. Uzun, O. Gunduz, Comparative characterization of the hydrogel added PLA/β-TCP scaffolds produced by 3D bioprinting, *Bioprinting* 13 (2019), e00046, <https://doi.org/10.1016/j.bioprint.2019.e00046>.
- [136] H.J. Jeon, M. Lee, S. Yun, D. Kang, K. ho Park, S. Choi, E. Choi, S. Jin, J.H. Shim, W.S. Yun, B.J. Yoon, J. Park, Fabrication and characterization of 3D-printed bicomposite scaffolds based on PCL and silanated silica particles for bone tissue regeneration, *Chem. Eng. J.* 360 (2019) 519–530, <https://doi.org/10.1016/jcej.2018.11.176>.
- [137] J. Wang, M. Yang, Y. Zhu, L. Wang, A.P. Tomsia, C. Mao, Phage nanofibers induce vascularized osteogenesis in 3D printed bone scaffolds, *Adv. Mater.* 26 (2014) 4961–4966, <https://doi.org/10.1002/adma.201400154>.
- [138] Y. Dong, J. Liang, Y. Cui, S. Xu, N. Zhao, Fabrication of novel bioactive hydroxyapatite-chitosan-silica hybrid scaffolds: combined the sol-gel method with 3D plotting technique, *Carbohydr. Polym.* 197 (2018) 183–193, <https://doi.org/10.1016/j.carbpol.2018.05.086>.
- [139] M. Ramu, M. Ananthasubramanian, T. Kumaresan, R. Gandhinathan, S. Jothi, Optimization of the configuration of porous bone scaffolds made of Polyamide/Hydroxyapatite composites using Selective Laser Sintering for tissue engineering applications, *Bio Med. Mater. Eng.* 29 (2018) 739–755, <https://doi.org/10.3233/BME-181020>.
- [140] C. Zhou, Bioactive ceramics and metals for regenerative engineering, in: *Regen. Eng. Adv. Mater. Sci. Princ.*, first ed., CRC Press, 2018, pp. 31–43, <https://doi.org/10.1201/9781315121079-3>.
- [141] J. Wilkes, Y. Hagedorn, W. Meiners, K. Wissenbach, Additive manufacturing of ZrO₂-Al203 ceramic components by selective laser melting, *Rapid Prototyp. J.* 19 (2013) 51–57, <https://doi.org/10.1108/13552541311292736>.
- [142] V.K. Balla, S. Bose, A. Bandyopadhyay, Processing of bulk alumina ceramics using laser engineered net shaping, *Int. J. Appl. Ceram. Technol.* 5 (2008) 234–242, <https://doi.org/10.1111/j.1744-7402.2008.02202.x>.
- [143] D. Sohrabi Baba Heidary, M. Lanagan, C.A. Randall, Contrasting energy efficiency in various ceramic sintering processes, *J. Eur. Ceram. Soc.* 38 (2018) 1018–1029, <https://doi.org/10.1016/j.jceramsoc.2017.10.015>.
- [144] B. Zhang, X. Pei, C. Zhou, Y. Fan, Q. Jiang, A. Ronca, U. D'Amora, Y. Chen, H. Li, Y. Sun, X. Zhang, The biomimetic design and 3D printing of customized mechanical properties porous Ti6Al4V scaffold for load-bearing bone reconstruction, *Mater. Des.* 152 (2018) 30–39, <https://doi.org/10.1016/j.matdes.2018.04.065>.
- [145] C.N. Kelly, J. Francovich, S. Julmi, D. Safranski, R.E. Guldberg, H.J. Maier, K. Gall, Fatigue behavior of As-built selective laser melted titanium scaffolds with sheet-based gyroid microarchitecture for bone tissue engineering, *Acta Biomater.* 94 (2019) 610–626, <https://doi.org/10.1016/j.actbio.2019.05.046>.
- [146] L. Zhao, X. Pei, L. Jiang, C. Hu, J. Sun, F. Xing, C. Zhou, Y. Fan, X. Zhang, Bionic design and 3D printing of porous titanium alloy scaffolds for bone tissue repair, *Compos. B Eng.* 162 (2019) 154–161, <https://doi.org/10.1016/j.compositesb.2018.10.094>.
- [147] A. Ataei, Y. Li, D. Fraser, G. Song, C. Wen, Anisotropic Ti-6Al-4V gyroid scaffolds manufactured by electron beam melting (EBM) for bone implant applications, *Mater. Des.* 137 (2018) 345–354, <https://doi.org/10.1016/j.matdes.2017.10.040>.
- [148] B. Wysocki, J. Idaszek, K. Szlak, K. Strzelczyk, T. Brynk, K. Kurzydowski, W. Święszański, Post processing and biological evaluation of the titanium scaffolds for bone tissue engineering, *Materials* 9 (2016) 197, <https://doi.org/10.3390/ma9030197>.
- [149] P. Caravaggi, E. Liverani, A. Leardini, A. Fortunato, C. Belvedere, F. Baruffaldi, M. Fini, A. Parrilli, M. Mattioli-Belmonte, L. Tomesani, S. Pagani, CoCr porous scaffolds manufactured via selective laser melting in orthopedics: topographical, mechanical, and biological characterization, *J. Biomed. Mater. Res. B Appl. Biomater.* 107 (2019) 2343–2353, <https://doi.org/10.1002/jbm.b.34328>.
- [150] Y. Li, J. Zhou, P. Pavanram, M.A. Leeflang, L.I. Fockaert, B. Pouran, N. Tümer, K.-U. Schröder, J.M.C. Mol, H. Weinans, H. Jahr, A.A. Zadpoor, Additively manufactured biodegradable porous magnesium, *Acta Biomater.* 67 (2018) 378–392, <https://doi.org/10.1016/j.actbio.2017.12.008>.
- [151] S. Limmahakun, A. Oloyede, K. Sitthiseripratip, Y. Xiao, C. Yan, 3D-printed cellular structures for bone biomimetic implants, *Addit. Manuf.* 15 (2017) 93–101, <https://doi.org/10.1016/j.addma.2017.03.010>.
- [152] C. Yan, L. Hao, A. Hussein, Q. Wei, Y. Shi, Microstructural and surface modifications and hydroxyapatite coating of Ti-6Al-4V triply periodic minimal

- surface lattices fabricated by selective laser melting, *Mater. Sci. Eng. C* 75 (2017) 1515–1524, <https://doi.org/10.1016/j.msec.2017.03.066>.
- [153] C. Vyas, H. Mishbak, G. Cooper, C. Peach, R.F. Pereira, P. Bartolo, Biological perspectives and current biofabrication strategies in osteochondral tissue engineering, *Biomanufacturing Rev* 5 (2020) 2, <https://doi.org/10.1007/s40898-020-00008-y>.
- [154] B. Zhang, J. Huang, R.J. Narayan, Gradient scaffolds for osteochondral tissue engineering and regeneration, *J. Mater. Chem. B* 8 (2020) 8149–8170, <https://doi.org/10.1039/DOTB00688B>.
- [155] S. Critchley, E.J. Sheehy, G. Cunniffe, P. Diaz-Payne, S.F. Carroll, O. Jeon, E. Alsberg, P.A.J. Brama, D.J. Kelly, 3D printing of fibre-reinforced cartilaginous templates for the regeneration of osteochondral defects, *Acta Biomater.* 113 (2020) 130–143, <https://doi.org/10.1016/j.actbio.2020.05.040>.
- [156] F. Gao, Z. Xu, Q. Liang, B. Liu, H. Li, Y. Wu, Y. Zhang, Z. Lin, M. Wu, C. Ruan, W. Liu, Direct 3D printing of high strength biohybrid gradient hydrogel scaffolds for efficient repair of osteochondral defect, *Adv. Funct. Mater.* 28 (2018), 1706644, <https://doi.org/10.1002/adfm.201706644>.
- [157] C. Wang, H. Yue, W. Huang, X. Lin, X. Xie, Z. He, X. He, S. Liu, L. Bai, B. Lu, Y. Wei, M. Wang, Cryogenic 3D printing of heterogeneous scaffolds with gradient mechanical strengths and spatial delivery of osteogenic peptide/TGF- β 1 for osteochondral tissue regeneration, *Biofabrication* 12 (2020), 025030, <https://doi.org/10.1088/1758-5090/ab7ab5>.
- [158] M. Barbeck, T. Serra, P. Booms, S. Stojanovic, S. Najman, E. Engel, R. Sader, C. J. Kirkpatrick, M. Navarro, S. Ghanaati, Analysis of the in vitro degradation and the in vivo tissue response to bi-layered 3D-printed scaffolds combining PLA and biphasic PLA/bioglass components – guidance of the inflammatory response as basis for osteochondral regeneration, *Bioact. Mater.* 2 (2017) 208–223, <https://doi.org/10.1016/j.bioactmat.2017.06.001>.
- [159] X. Zhou, T. Esworthy, S.-J. Lee, S. Miao, H. Cui, M. Plesiniak, H. Fenniri, T. Webster, R.D. Rao, L.G. Zhang, 3D Printed scaffolds with hierarchical biomimetic structure for osteochondral regeneration, *Nanomed. Nanotechnol. Biol. Med.* 19 (2019) 58–70, <https://doi.org/10.1016/j.nano.2019.04.002>.
- [160] S. Vijayaventaraman, W.F. Lu, J.Y.H. Fuh, 3D bioprinting of skin: a state-of-the-art review on modelling, materials, and processes, *Biofabrication* 8 (2016), 032001, <https://doi.org/10.1088/1758-5090/8/3/032001>.
- [161] M. Albanna, K.W. Binder, S.V. Murphy, J. Kim, S.A. Qasem, W. Zhao, J. Tan, I. B. El-Amin, D.D. Dice, J. Marco, J. Green, T. Xu, A. Skardal, J.H. Holmes, J. D. Jackson, A. Atala, J.J. Yoo, In situ bioprinting of autologous skin cells accelerates wound healing of extensive excisional full-thickness wounds, *Sci. Rep.* 9 (2019) 1856, <https://doi.org/10.1038/s41598-018-38366-w>.
- [162] B.S. Kim, G. Gao, J.Y. Kim, D. Cho, 3D cell printing of perfusable vascularized human skin equivalent composed of epidermis, dermis, and hypodermis for better structural recapitulation of native skin, *Adv. Healthc. Mater.* 8 (2019), 1801019, <https://doi.org/10.1002/adhm.201801019>.
- [163] P. Admane, A.C. Gupta, P. Jois, S. Roy, C. Chandrasekharan Lakshmanan, G. Kalsi, B. Bandyopadhyay, S. Ghosh, Direct 3D bioprinted full-thickness skin constructs recapitulate regulatory signaling pathways and physiology of human skin, *Bioprinting* 15 (2019), e00051, <https://doi.org/10.1016/j.bprint.2019.e00051>.
- [164] A. Desanlis, M. Albouy, P. Rousselle, A. Thépot, M.D. Santos, C. Auxenfans, C. Marquette, Validation of an implantable bioink using mechanical extraction of human skin cells: first steps to a 3D bioprinting treatment of deep second degree burn, *J. Tissue Eng. Regen. Med.* (2020) 3148, <https://doi.org/10.1002/term.3148>, term.
- [165] Y. Huyan, Q. Lian, T. Zhao, D. Li, J. He, Pilot study of the biological properties and vascularization of 3D printed bilayer skin grafts, *Int. J. Bioprinting*. 6 (2020), <https://doi.org/10.18063/ijb.v6i1.246>.
- [166] P. Liu, H. Shen, Y. Zhi, J. Si, J. Shi, L. Guo, S.G. Shen, 3D bioprinting and in vitro study of bilayered membranous construct with human cells-laden alginate/gelatin composite hydrogels, *Colloids Surf. B Biointerfaces* 181 (2019) 1026–1034, <https://doi.org/10.1016/j.colsurfb.2019.06.069>.
- [167] D.-C. Guo, C.L. Papke, R. He, D.M. Milewicz, Pathogenesis of thoracic and abdominal aortic aneurysms, *Ann. N. Y. Acad. Sci.* 1085 (2006) 339–352, <https://doi.org/10.1196/annals.1383.013>.
- [168] P. Danyi, J.A. Elefteriades, I.S. Jovin, Medical therapy of thoracic aortic aneurysms: are we there yet? *Circulation* 124 (2011) 1469–1476, <https://doi.org/10.1161/CIRCULATIONAHA.110.006486>.
- [169] E.M. Isselbacher, Thoracic and abdominal aortic aneurysms, *Circulation* 111 (2005) 816–828, <https://doi.org/10.1161/01.CIR.0000154569.08857.7A>.
- [170] S.H. Ellozy, A. Carroccio, M. Minor, T. Jacobs, K. Chae, A. Cha, G. Agarwal, B. Goldstein, N. Morrissey, D. Spielvogel, R.A. Lookstein, V. Teodorescu, L. H. Hollier, M.L. Marin, Challenges of endovascular tube graft repair of thoracic aortic aneurysm: mid-term follow-up and lessons learned, *J. Vasc. Surg.* 38 (2003) 676–683, [https://doi.org/10.1016/S0741-5214\(03\)00934-0](https://doi.org/10.1016/S0741-5214(03)00934-0).
- [171] M.L. Marin, L.H. Hollier, S.H. Ellozy, D. Spielvogel, H. Mitty, R. Griep, R. A. Lookstein, A. Carroccio, N.J. Morrissey, V.J. Teodorescu, T.S. Jacobs, M. E. Minor, C.M. Sheahan, K. Chae, J. Oak, A. Cha, Endovascular stent graft repair of abdominal and thoracic aortic aneurysms: a ten-year experience with 817 patients, *Trans. Meet. Am. Surg. Assoc.* 121 (2003) 279–288, <https://doi.org/10.1097/01.sla.0000090473.63393.e9>.
- [172] C. Kucukgul, S.B. Ozler, I. Inci, E. Karakas, S. Irmak, D. Gozuacik, A. Taralp, B. Koc, 3D bioprinting of biomimetic aortic vascular constructs with self-supporting cells, *Biotechnol. Bioeng.* 112 (2015) 811–821, <https://doi.org/10.1002/bit.25493>.
- [173] E. Yeung, T. Fukunishi, Y. Bai, D. Bedja, I. Pitaktong, G. Mattson, A. Jeyaram, C. Lui, C.S. Ong, T. Inoue, H. Matsushita, S. Abdollahi, S.M. Jay, N. Hibino, Cardiac regeneration using human-induced pluripotent stem cell-derived biomaterial-free 3D-bioprinted cardiac patch in vivo, *J. Tissue Eng. Regen. Med.* 13 (2019) 2031–2039, <https://doi.org/10.1002/term.2954>.